University of Stavanger

Faculty of Science and Technology

MASTER'S THESIS

Study programme/ specialisation: M.Sc., Petroleum Technology/ Reservoir Engineering	Autumn semester, 2020 Open
Author: Temidayo Olayinka Boboye	…… (signature of author)
Supervisor(s): Pål Østebø Andersen	
Title of master's thesis: An Improved Approach in Estimating Gas Permeability for Tight Reservoir Rocks.	
Credits (ECTS): 30	
Keywords: Unconventional reservoirs Gas properties Desorption/Adsorption Permeability	Number of pages: 50 Stavanger, 15.12.2020

Abstract

The impact of the permeability on ultra-tight porous media influences flow behaviour inside the media. The unconventional reservoir gas permeability significantly impacts rock property estimation crucial to unconventional resource development. The rock permeability describes how unconventional reservoir gas flows into the pores, which affects reservoir development. The pressure decay approach estimates the permeability of unconventional rocks by evaluating the pressure difference in reservoirs. Due to the pulsed pressure decay method's effectiveness over the laboratory run time, the analytical solutions determine the permeability. The analytical method to determine the permeability relied on the simulated pressure results, which have limitations in estimating permeability based on constant gas properties. There will be changes between the experimental pressure and the simulated pressure results because these curves have similar late slopes for the estimated permeability. This study aims to eliminate the large differences with inconsistent results between the experimental pressure results' historical matching and those of the simulated pressure results.

A representation of a mathematical model containing gas characteristics related to pressure was developed. When the minimum difference between the experimental pressure and the simulated pressure results stabilizes, the permeability estimation occurs. This study's approach estimated permeability from pulse pressure decay, using laboratory data by testing three gases that include Methane, Helium, and carbon dioxide. This new approach measures the slightest variation in the pressure decay response evaluation based on history matching. This method estimated permeability more accurately when compared with the Cui et al. (2009) analytical solution. The improved estimation of gas permeability in this study was due to the applicability of pressure-dependent gas properties and the entire pressure outcome's implementation to represent pressure decay dynamics. The sensitivity analysis shows that implementing the entire pressure outcome to represent the dynamics of pressure decay is significant in estimating permeability. In contrast, variation in porosity, Langmuir pressure, and Langmuir volume are less significant in the permeability estimation, making the pulse pressure decay approach for estimating permeability to be valid.

Simulated pressure means the endmost equilibrium pressure for each pressure step and typifies similar pressure to determine permeability.

Acknowledgment

I am indebted to my supervisor for his support, excellent guidance, patience, and motivation throughout this research.

Special thanks to the Department of Petroleum Resources to release the data used in this entire study. I am indeed grateful to my parents, who have continuously encouraged and inspired me to excel in everything I do. I want to thank my brother, Engr Temitope Boboye, for being a brother to me always. I warmly thank my only sister, Mrs. Temiloluwa Akinwande, for her support. A special thanks to my younger brother, Mr. Temitayo Boboye, for all the innovative ideas. I am indebted to my fiancée for the perfect understanding she puts forward always. I am grateful to have a more prominent family of RCCG Dayspring Stavanger.

I am grateful to Petroleum Technology Development Funds for the opportunity that makes this dream a reality. It is a rare privilege to have good friends around me throughout my studies. I am thanks for the care and support from my roommate and co-recipient, Nonso Ihebuzor, and my friends: Ebuka Okoli (Rev. Father), Obinna Eleri, Nasir Baba Lawan Jr (Alhaji), Iida, Kevin Stanley, Atul Giri, and all GG3 past and recent residents.

Simulated pressure means the endmost equilibrium pressure for each pressure step and typifies similar pressure to determine permeability.

Table of Contents

Simulated pressure means the endmost equilibrium pressure for each pressure step and typifies similar pressure to determine permeability.

Simulated pressure means the endmost equilibrium pressure for each pressure step and typifies similar pressure to determine permeability.

List of Figures

Figure A- 1: Flowchart for the conversion of density to pressure..... 48

Simulated pressure means the endmost equilibrium pressure for each pressure step and typifies similar pressure to determine permeability.

List of Tables

Simulated pressure means the endmost equilibrium pressure for each pressure step and typifies similar pressure to determine permeability.

Nomenclature

A = Area of the sample, m^2

K = Permeability, mD

ΔP = Pressure difference between upstream and downstream reservoirs, Psi

L = Length of sample, m

U = Darcy velocity, m/s

μ_g = Viscosity, Pa.s

∂P = Differential pressure

∂x = Differential distance

C_e = Adsorbed gas volume, m^3

R = Universal gas constant, J/kg mol

M = Molar mass, g/mol

P = Gas pressure, Psi

P_g = Gas pressure, Pa

P_L = Langmuir half capacity pressure, Pa

T = Temperature, K

V= Volume, m^3

P_i = Initial pressure, Pa

K_a = Apparent permeability, mD

K_∞ = Intrinsic permeability, mD

K_n = Knudsen number

R = Universal gas constant, J/kg mol

T_{res} = Reservoir temperature, Kelvin

M = Gas molar mass, Kg/mol

r = Radius pore size, nm

P_L = Langmuir pressure, Pa

Simulated pressure means the endmost equilibrium pressure for each pressure step and typifies similar pressure to determine permeability.

q_L = Langmuir volume, m^3

ϕ = Porosity

C_g = Gas compressibility, Psi^{-1}

s_1 = Difference in upstream and downstream pressures slope on a semi-log

V_d = Volume of downstream reservoir, m^3

V_u = Volume of upstream reservoir, m^3

f_1 = Correction factor

a, b = denotes volume correlation of pore relative to downstream and upstream reservoir volumes.

V_{std} = Volume of sample.

P_u = Upstream pressure, Psi

P_d = Downstream pressure, Psi

C = Density adsorption per unit density of the rock

ρ = Density, Kg/m^3

Simulated pressure means the endmost equilibrium pressure for each pressure step and typifies similar pressure to determine permeability.

Chapter One

Introduction

As an unconventional reservoir, unconventional gas reservoirs have different geological and physical properties from conventional reservoirs. Permeability is an important intrinsic factor during gas production, carbon sequestration. Permeability depends on the distribution of the pore size and its geometry. The importance of the accurate estimation of permeability in a porous media either for a multiphase or single-phase flow and the connection between the saturation, pressure cannot be overemphasized. The approach in this project is placed in the context of review existing pressure decay measurement methods. The latter part of this chapter explains the research objectives, problem statement, literature review, and thesis outline.

1.1 Background

The energy demand is on a global exponential increase with more projections toward clean and environment-friendly resources. Resources with non-traditional production approaches include coal bed methane, shale gas, tight reservoirs, and heavy oil. Unconventional reservoirs are gaining exploitation due to high energy demand. The recent technological advancement and continuous decline in production with the lack of significant discovery of conventional reservoirs have positioned unconventional resources as the potential alternative. The distinctive character of unconventional resources is the ultra-low permeability of varying magnitudes that define the fluid flow and its interactions with rock surfaces.

In unconventional gas reservoirs, the matrix's pore size varies from 1 nm and 100 nm (Loucks et al. (2009)). It enables permeability testing due to non-Darcy flow in the unconventional gas reservoir (Darabi, Ettehad, & Javadpour, 2012). The movement of gas through the rock matrix is by either Darcy flow(advection) or diffusion. The complexity of unconventional reservoir gas movement makes it difficult to measure all the essential components contributing to optimized production fully. The complexity is evident by the co-existence of different flow regimes in the unconventional reservoir (Javadpour F., 2009). A potential inaccurate value of permeability occurred when conventional Darcy's flow is considered during permeability testing (Cui, Bustin, & Bustin, 2009). It is challenging to determine permeability in unconventional reservoirs by laboratory methods due to the inability to attain a steady-state flow; also, the low flow rates measured with high inaccuracy (Hsieh et al. (1981)); (Finsterle & Persoff, 1997). There is a high potential risk of damage to tight rocks with the application of high volumes of fluids during the conventional measurement process (Amaefule et al. (1986)).

Simulated pressure means the endmost equilibrium pressure for each pressure step and typifies similar pressure to determine permeability.

Permeability evaluation is by both transient and steady-state approaches for tight rocks. Gas slippage describes the difference between liquid and gas (Tanikawa & Shimamoto, 2009). The measurement of the permeability in unconventional reservoirs involves using a transient pulse-decay approach (Han et al. (2019)). The pulse-decay method was initially used to measure granite's permeability (Brace et al. (1968)), though the gas's fluid compressibility was neglected. Brace et al. (1968) developed fully integrated analytical solutions that accounted for fluid compressibility storage effects relative to hydraulic head and pressure.

The gas compressibility is the ratio of the change in gas volume to the corresponding change in pressure at a constant temperature. The gas compressibility is higher with better compressibility storage effects compare to that of liquid. (Ning, 1992) obtained permeability for fractured and un-fractured cores by history matching their pressure curves with an in-house built simulator. The operational complexity entails the exclusion of some intrinsic factors such as gas compressibility, use of large upstream and downstream reservoirs compares to the pore volume of the analytical solutions of Hsieh et al.'s work. The elimination of the operational complexity involves using an approximate analytical solution approach that yielded accurate results with smaller upstream and downstream volumes than pore volume (Dicker & Smits, 1988).

1.2 Attributes of Unconventional Gas Reservoirs

The deposition of the unconventional reservoir is below sea level of dead organism emergence because of gradual simultaneous accumulation and precipitation of clay particle, carbonates with biotic residue with limited access to a circulation of water and air. Unconventional reservoir gas differs from conventional reservoirs in various ways. The rock in the unconventional reservoir is both the sealing and source rock that prevents the gas from migrating to the surface and store rich organic content. Gas can be stored in ultra-tight unconventional reservoir formations both as free gas in porous spaces and natural fractures of the unconventional reservoir rock and absorbed gas within organic material (Cipolla & Lolon, 2010). Unconventional reservoirs have very low permeability. The effective permeability of unconventional reservoir ranges from $10^{-3}$to 10^{-6} mD. When producing from the unconventional reservoirs, the hydraulic fracture created a flow path at the near wellbore. Productivity from unconventional reservoirs is a function of fracture conductivity and an unconventional reservoir's source rock's original permeability.

The hydrocarbon kitchen of the unconventional reservoir consists of reservoir rocks and source rocks. The unconventional gas reservoir has a trapping mechanism like conventional reservoirs. However, the unconventional hydrocarbons are exploited through and at the source rock (inside the rock where the

Simulated pressure means the endmost equilibrium pressure for each pressure step and typifies similar pressure to determine permeability.

generation occurs). There are different gas storage processes in unconventional gas reservoirs, namely, compressed free gas in nanoscale pores in the organic matter and dissolved gas in the kerogenic material (Javadpour, Fisher, & Unsworth, 2007). The flowability of the unconventional gas reservoir is dependent on the matrix and fracture structures of the reservoir. Matrix constituents are lithified clays, detrital minerals, and organic material, where the latter is an essential constituent of a productive unconventional gas reservoir (Moghanloo, Javadpour, & Davudou, 2013).

1.3 Flow Mechanisms in Unconventional Reservoirs

The flow of gas in an unconventional reservoir is dependent on diffusion and Darcy flow. The gas will flow due to pressure differential. The flow of gas is mostly dependent on porosity and permeability in hydrocarbon reservoirs. Gas flow in unconventional reservoirs is through nanopore size with high velocity, which accounts for gas slippage effects. The quantification of the gas adsorption is by the amount of gas that is resident on the kerogen's surface, which changes pore pressure changes. Gas adsorption slows down transport processes and impacts the final pressure for a steady state. Gas compressibility influences the pressure difference.

1.3.1 Flow Regime

Gas transport in porous media has four flow regimes according to the Knudsen number (as shown in Table 1), the explanation is by (Liehui, 2019).

1) Continuum flow regime occurs at Knudsen number below 0.001 when there is a higher collision chance between the gas pore size and the media and pore walls. The flow of gas is controlled by viscous flow, while Knudsen diffusion is negligible.
2) A slip flow regime occurs when Knudsen's number ranges between 0.001 and 0.1. This flow is characterized by the larger pore size of the medium against that of gas molecules, with higher collisions that are significant. Therefore, although viscous flow is still the dominant mechanism, Knudsen diffusion affects gas transport and cannot be ignored. In this regime, the Darcy equation fails to describe the gas transport in porous media.
3) Transition regime occurs when Knudsen's number ranges from 0.1 to 10. At this regime, the porous media's pore size is the same as that of gas molecules, with pore walls collisions. The description of the gas flow is by Knudsen diffusion and viscous flow.
4) When Knudsen's number is above 10, then a free molecule regime occurs. The collision is higher between molecules than between molecules and pore walls due to the smaller pore size of gas molecules. The gas flow dominance is by Knudsen diffusion.

Simulated pressure means the endmost equilibrium pressure for each pressure step and typifies similar pressure to determine permeability.

The unconventional reservoir matrix's primary pore size is less than 1µm to illustrate the unconventional reservoir nanopores' gas transport regime. Fig. 4 shows the variations of the Knudsen number with pressure at different pore diameters. From figure 4, the Knudsen number ranges between 0.001 and 10 for corresponding pressure from 0.1 to 10MPa at pore diameter that is less than 1 µm. Hence, the central gas transport regime of unconventional reservoir nanopores are slip flow and transition regimes. Both the viscous flow and the Knudsen diffusion significantly impact gas transport in nanopores. The Darcy equation cannot describe gas transport in nanopores. However, the slip and transition flow regimes are most likely to be encountered in most unconventional gas reservoirs because the Knudsen number Kn in most unconventional reservoirs lies between 0.001 to 1 (Ziarani, 2012).

1.3 Problem Statement

Determination of the permeability of unconventional gas reservoirs is essential for production optimization. Dynamic changes in the pore pressure account for gas that can be absorbed in the kerogen's surface. The large surface area of the kerogen is essential in quantifying gas absorption. How does the adsorption/ desorption contribute to the accurate determination of the permeability in unconventional gas reservoirs? The nanopore size of the porous medium through which non-Darcy flows describe gas moves. What is the impact of the gas slippage effect on the determination of permeability, or can its effects be neglected during pulse decay tests? The compressibility of the gas may be another factor that impacts the permeability of the unconventional gas reservoir. To what extent are the contributing effects of gas compressibility relevant to production? There is a need to establish how compressibility, gas slippage, and absorption/desorption collectively contribute to optimized production. How can a systematic design, application, and alteration of these intrinsic factors affect unconventional gas output? How relevant is this in establishing a non-Darcy type of flow?

1.4 Research Focus

This research aims to

- Develop a numerical model for pulse decay measurement of permeability.
- Determination of permeability and how slippage effect impacts.
- Investigation of systematically varied contribution of the intrinsic factors during estimation of permeability
- Investigate gas slippage interactions, adsorption/desorption, and gas compressibility effects that contribute to accurate estimation of permeability.

1.5 Outcomes of Study

The research contribution will look at the following:

Simulated pressure means the endmost equilibrium pressure for each pressure step and typifies similar pressure to determine permeability.

- Investigate the effects of various contributing/ controlling factors on the determination of permeability.
- Develop a comprehensive reservoir model simulation that gives an accurate determination of permeability by incorporating all essential controlling factors.
- Propose an improved, efficient, and reliable approach for estimating permeability.

1.6 Conspectus of Thesis

This project puts forward an extensive model with the incorporated desorption/adsorption and gas compressibility storage effect. The modeling of the gas surface assimilation is by Langmuir isotherm. The simulator's development on MATLAB simulates permeability through the permeability pulse decay approach and the impacts of contributing intrinsic factors.

Chapter 2 present the flow model and review the theoretical and experimental pulse decay measurement of permeability. It explains the complex physics of unconventional gas reservoirs and gives a better insight into the intrinsic factors that affect the permeability measurement in unconventional reservoirs.

Chapter 3 presents the numerical model development involved in the gas compressibility storage effects and desorption of unconventional gas reservoirs. It utilizes the robust programming language of MATLAB for the simulation.

Chapter 4 presents the simulation results generated through MATLAB. The results discussed considering systematic sensitivity analysis of the intrinsic factors.

Chapter 5 presents the conclusion of the project.

The next chapter accounts for the project's references, and the appendix presents MATLAB code, input data file, and a generated output data file in MATLAB simulator.

Simulated pressure means the endmost equilibrium pressure for each pressure step and typifies similar pressure to determine permeability.

Chapter Two

Literature Review

This chapter gives an overview of the problem studied in this work and provides the relevant theoretical background.

2.1 Darcy Law

Darcy's law for single-phase gas flow as described by (Darcy 1856):

$$Q = \frac{KA}{\mu_g}\frac{\Delta \mathrm{P}}{L} \tag{1}$$

For one-directional flow parallel to the x-axis, the differential form is:

$$u = \frac{Q}{A} = -\frac{K}{\mu_g}\frac{\partial P}{\partial x} \tag{2}$$

Pressure difference relative to the flow direction is accounted for by negative signs (Peaceman, 1977). Gas flow in unconventional reservoirs is modeled based on Darcy's law.

2.2 Gas Diffusion

The dominant continuum regime that exists in the unconventional reservoirs depends on the ultra-tight pore structures.

The variation in flow regimes of ultra-low reservoirs results from the effective change in unconventional reservoir permeability. This change in the flow regime decreases reservoir pressure, decreasing pore pressure with increasing apparent permeability, which leads to gas production enhancement in recovery (Javadpour, 2009).

(Xu, Haghighi, & Cooke, 2012) suggested Green's model approach that estimates production fractures in horizontal well at a transient state flow regime for ultra-low gas reservoirs. While (Michel, Villazon, R., Civian, & Devegowda, 2011) investigated the various flow regimes for both ideal and real gases for gas transportation in nanoscale porous media with consideration of pore size effects.

Typical gas diffusion occurs with the gas collides with the wall membranes and with each other; likewise, it is Knudsen diffusion, though the collision of the gases is with pore walls. Identifying the flow regime is based on the Knudsen number - a dimensionless parameter that measures Knudsen diffusion's degree (Wang & Marongiu-Porcu, 2015). The proportion of the mean free path to the length depends on the length of the channel defines Knudsen number, which in the case of unconventional gas reservoirs is the effective pore radius, r (Knudsen, 1909):

$$K_n = \frac{\lambda}{r} \tag{3}$$

The mean free path relationship was put forward as (Civan, Rai, & Sondergeld, 2011)

Simulated pressure means the endmost equilibrium pressure for each pressure step and typifies similar pressure to determine permeability.

$$\lambda = \frac{\mu_g}{P}\sqrt{\frac{\pi R T_{res}}{2M}} \quad (4)$$

μ_g is the viscosity of the gas, T, and P are bottom-hole temperature and pressure.

Introduce a real-gas Z-factor into equation (4), which gives:

$$K_n = \frac{\mu_g Z}{P\, r}\sqrt{\frac{\pi R T_{res}}{2M}} \quad (5)$$

Table 1 is a detailed explanation of using Knudsen number ranges to classify the different flow regimes that can occur in unconventional gas reservoirs. Ziarani and Aguilera said the flow regimes for most unconventional gas reservoirs range from $0.001 - 1$ Knudsen.

Table 1: Flow regimes determination by Knudsen number K_n.

Knudsen Number	Flow Regime	Criteria	Dominant Mechanism
$\mathbf{10^0 - 10^{-3}}$	**Continuum**	**MFP < Pore Size**	**Darcy**
$\mathbf{10^{-3} - 10^{-1}}$	**Slip**	**MFP > Pore Size**	**Non-Darcy**
$\mathbf{10^{-1} - 10^{1}}$	**Transition**	**MFP = Pore Size**	**Viscous**
$\mathbf{> 10^{1}}$	**Free molecule**	**MFP < Pore Size**	**Knudsen Flow**

MFP= Mean Free

2.3 Permeability

Darcy's law does not fully capture the full description of actual gas characteristics and transportation in nanopores network. A developed relationship calculates the mean free path in equation (4), and substituting the mean free path by including real gas, Z-factor yields the following relationship in equation (5) (Civan, Rai, & Sondergeld, 2011). However, the Knudsen number Kn in most unconventional reservoirs lies between $0.001\ to\ 1$ (Ziarani & Aguilera, 2012), which indicates that the slip and transition flow regimes are most likely to be encountered in most unconventional gas reservoirs. The apparent permeability of the matrix of the unconventional reservoir is:

$$K_a = K_\infty f(K_n) \quad (6)$$

K_∞ is the medium permeability, and $f(Kn)$ relates apparent and intrinsic matrix permeability. Different models have been developed, based on experiments, to quantify the relationship between intrinsic permeability and nanopore structure in porous media (Beskok & Karniadakis, 1999). For a capillary tube of radius, r, the intrinsic permeability can be derived from equation (14) in Beskok and Karniadakis (1999):

$$K_\infty = \frac{128\pi^2}{15} tan^{-1}\left(4{K_n}^{0.4}\right) \quad (7)$$

Simulated pressure means the endmost equilibrium pressure for each pressure step and typifies similar pressure to determine permeability.

The matrix intrinsic permeability K_∞ is related to the nanopore geometry that allows fluid flow effectively. A correlation developed for $f\ (K_n)$ based on extensive laboratory experiments for improved permeability regime transition (Sakhaee-Pour & Bryant, 2012):

$$f\ (K_n) = \begin{cases} 1 + 5K_n & \text{Slip Regime} \quad 10^{-3} - 10^{-1} \\ 0.8453 + 5.4576K_n + 0.1633k_n^2 & \text{Transition Regime} \quad 0.1 < K_n < 0.8 \end{cases} \tag{8}$$

$$K_a = \frac{\phi\, r^2}{8\tau}(1 + K_\infty\, K_n)\left(1 + \frac{4K_n}{1 + K_n}\right) \tag{9}$$

Intuitively, equations (5) and (8) predict net increases of K_n, and $f\ (K_n)$ is defined with reduced pore pressure.

The ultra-low permeability of rocks is determined in the laboratory using the three most common methods of gas injection, including core analysis, crushed sample analysis, and mercury intrusion curves from mercury porosimetry. Although, conventional resource permeability is determined using rock core under confined conditions. Another means of measuring permeability is steady flow permeability measurement in unconventional reservoirs. However, this approach has limitations because of time scales and instrumentation constraints to measure the minute difference in flow rate and pressure drops (American Petroleum Institute, 1998). Measurement of permeability using mercury porosimeter with mercury injection relative to the relationship between mercury saturation and capillary pressure (Swanson, 1981).

2.4 Gas Compressibility

Isothermal gas compressibility determines the compressible properties of the reservoir. Gas is the most compressible element in porous media. Gas compressibility defines the relative change in the gas volume to the change in pressure at a constant temperature. The gas compressibility is expressed by:

$$C_g = \frac{-1}{V}\left(\frac{\partial V}{\partial P}\right) \tag{10}$$

The real gas compressibility expressed as:

$$C_g = \frac{1}{P} \tag{11}$$

The compressibility of a real gas written as:

$$C_g = \frac{1}{P} - \frac{1}{Z}\left(\frac{\partial z}{\partial P}\right)_T \tag{12}$$

By the real gas expression, it is evident that at low pressures, gas behaves as an ideal gas when the compressibility factor derivative to pressure sets to zero, and the gas compressibility conforms to an ideal gas. When pressures are low, gas compressibility is very high, resulting in a gas expansion to occupy a large volume at low pressure. At high pressures, gas compressibility reduces and results in liquid compressibility.

Simulated pressure means the endmost equilibrium pressure for each pressure step and typifies similar pressure to determine permeability.

2.5 Desorption / Adsorption

Unconventional resources comprise organic decay materials and kerogen. Gas in these resources can exist as free gas or absorbed gas (stored in pore networks). There is an increase in the release of absorbed gas as production increases with decreasing pressure. Langmuir isotherm adsorption describes desorbed gas, which accounts for a possible releasable amount of gas relative to the pressure in the pores.

$$C_e = \frac{q_L \ P}{P + P_L} \tag{13}$$

C_e is the adsorbed gas volume, P .L. and q_L are Langmuir pressure and Volume in psi and m^3.

During the exploitation of an unconventional gas reservoir, the following parameters are of importance, which includes Langmuir parameter values, desorption pressure, and gas storage volume. Gas desorption plays a vital role in the unconventional reservoir gas production recovery. Unconventional rock absorbs a large amount of gas on its formation surface. Mainly, methane absorbs on kerogen, and its absorption is quantified using Total Organic Content (TOC). More gas adsorption as production takes place with depleting pressure.

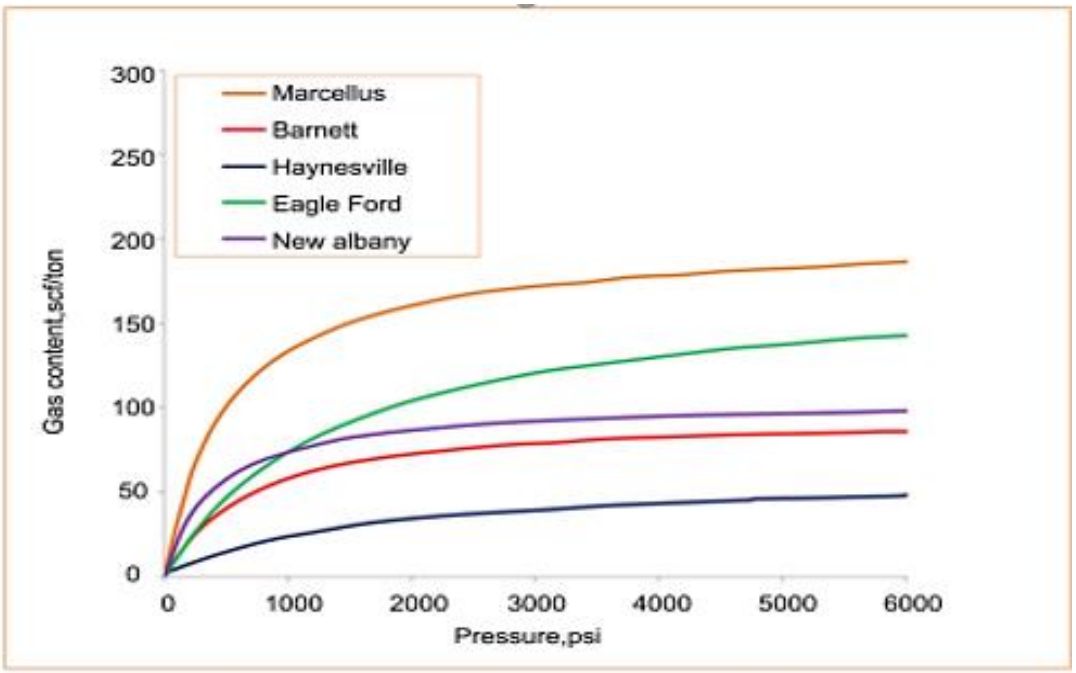

Figure 1: Adsorption Isotherms for different unconventional formation in the US

2.6 Previous Research

Based on the previous research works, Cui et al. (2009) developed a modified analytical solution to the usual determination of permeability, resulting in an inaccurate permeability value because of

Simulated pressure means the endmost equilibrium pressure for each pressure step and typifies similar pressure to determine permeability.

adsorption term exclusion. The incorporation of the sorption term into the various corresponding governing equations gives a better result. Therefore, permeability is determined analytically by:

$$K = \frac{-s_1 \mu C_g \ L}{f_1 A \left(\frac{1}{V_u} + \frac{1}{V_d}\right)} \tag{14}$$

s_1 is the difference in upstream and downstream pressures slope on a semi-log. To fully replicate Cui et al.'s analytical solution, the slope of the pressure on semi-log is s_1. Equation 14 is valid for a minimal pressure difference between the upstream and downstream reservoirs at lower reservoir volume ratios.

$$f_1 = \frac{{\theta_1}^2}{a + b} \tag{15}$$

f_1 is the correction factor for mass flow by Jones' (1997) model.

$$\tan\theta = \frac{(a + b)\theta}{\theta^2 - ab} \tag{16}$$

$$a = \frac{V_p}{V_u} \ ; \ \ b = \frac{V_p}{V_d} \tag{17}$$

a and b denotes volume correlation of pore relative to downstream and upstream reservoir volumes. The storage capacity of the sample when methane and carbon dioxide are considered based on the adsorptive property as:

$$a = \frac{V_p \left(1 + \frac{\phi_a}{\phi}\right)}{V_u} \ ; \ \ b = \frac{V_p \ \left(1 + \frac{\phi_a}{\phi}\right)}{V_d} \tag{18}$$

$$\phi_a = \frac{\rho_s (1 - \ \phi) q_L P_L}{V_{std} \ C_g \rho (P_L \ + P)^2} \tag{19}$$

2.7 Pulse-Decay Techniques

The complexity of the unconventional reservoirs demands distinctive techniques for ultra-low permeability determination with high accuracy. The traditional method of determining permeability is the steady-state approach that uses pressure drop and a constant flow rate. However, this approach

Simulated pressure means the endmost equilibrium pressure for each pressure step and typifies similar pressure to determine permeability.

fails in unconventional reservoirs because the lower flow rate is difficult to measure. The permeability of the rock core evaluation is under confined conditions. The inadequacy of the conventional methods of estimating permeability necessitates modifying the existing measurement approach to a more robust approach in determining the permeability of ultra-low rocks in the laboratory.

The most common methods for determining ultra-low permeability in unconventional reservoirs are:

- Transient Techniques
- Core Sample Analysis
- Crushed Sample Analysis
- On-site desorption Test of drill Cores or Cuttings
- Use of Mercury, Nitrogen, or Methane Porosimetry

1. Transient/ Unsteady/Pulse Decay Techniques: This technique estimates the permeability for ultra-low permeability reservoirs. Figure 4 shows the experimental layout in which the system's initial pressure is at equilibrium with the closure of the main valve. Gas flows into the system causes increased upstream pressure once the main valve is open. Pulsating pressure is measured both upstream and downstream as a function of gas flow by transducers. The pressure profiles from the upstream and downstream determine the permeability once equilibrium occurs in the system.

The pressure difference between the upstream and downstream reservoirs is given by:

$$dP(t) = \frac{P_u(t) - P_d(t)}{P_u(0) - P_d(0)} \tag{19}$$

Simulated pressure means the endmost equilibrium pressure for each pressure step and typifies similar pressure to determine permeability.

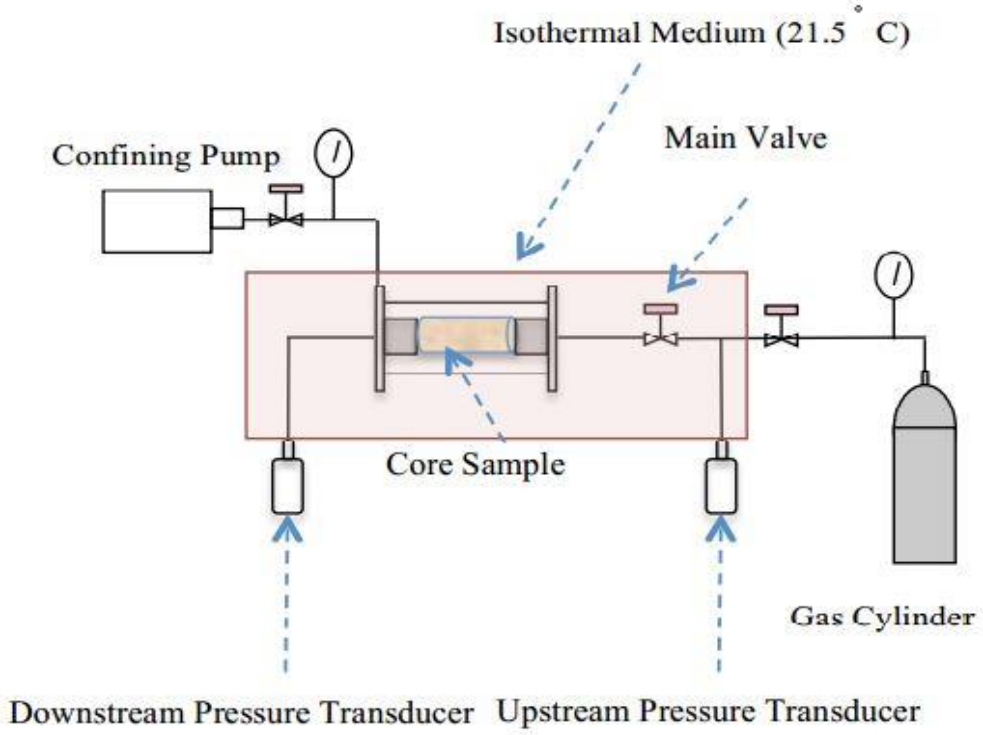

Figure 2: Experiment set-up for pressure pulse-decay permeability measurement (Alnoaimi & Kovscek, 2013).

2. Core Sample Analysis: The core sample plugs' conditioning is under confining reservoir stress, and permeability estimation are with the pressure pulse-decay method. Such samples are a good representative of the initial permeability in the unconventional reservoir. For a quicker permeability measurement determination, use a small thin disc for ultra-low permeability rocks in the laboratory. The measured permeability in this method is less than the actual permeability.
3. Crushed Sample Analysis: The sample used in this method is the crushed quasi-spherical sample—a similar apparatus as the core sample analysis approach. The experimental set-up has a reference cell filled with high-pressure gas and an experimental cell containing the spherical sample with a uniform radius. The high-pressure gas from the reference cell is released into the spherical samples at a given pressure. At equilibrium, the reference cell and void Volume of the experimental cell have equal pressure. The gas in the experimental cell permeates through the ultra-low permeability rock samples until pressure is at equilibrium in the void volume and pore space. Record the pressure decay pulses in the experimental cell. The use of gas expansion on crushed samples under the original confining stress state of the reservoirs is not pragmatic. The secondary fractures and large pores break into smaller crushed sample sizes; therefore, this method measured permeability mainly from primary nanopores. The permeability of the hydraulically fractured reservoir is responsive relative to rock stress,

Simulated pressure means the endmost equilibrium pressure for each pressure step and typifies similar pressure to determine permeability.

unlike crushed sample permeability. Changes occur in equivalent permeability of experimental or reservoir pressures against the expected permeability from stress-dependent because the permeability of crushed samples is a representative of the transport properties of the unfractured reservoir or undamaged matrix of fractured reservoirs. It is complex and challenging to perform experiments at varying pressures.

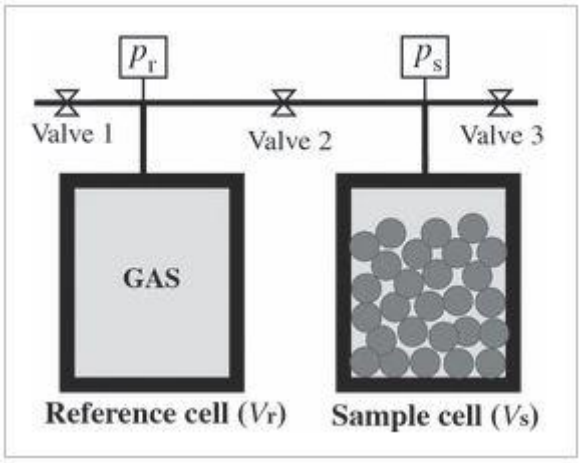

Figure 3 (Cui et al. *(2009)*): An experimental set-up of crushed sample method in determining permeability.

4. On-site desorption Test of drill Cores or Cuttings: The permeability estimate from this method is without confining pressure, though it is like that of the crushed sample method. Remove the confining pressure once the core gets to the surface, and fractures induced on the cores with possible re-sealing. This method of estimating permeability preserves the gas in the primary micro-pores. It seals the core in the desorption canister making the micro-pores of the undamaged matrix. The gas used in this method is natural gas from the reservoir as against nitrogen, mercury, or pure methane as used by other methods.
5. Use of Mercury, Nitrogen, or Methane Porosimetry: For natural gas reservoir, the main composition element is methane. The complexities of the micro-pores network and strong selective transport properties of different gases in the ultra-low permeability rock due to intensive gas molecules and pores interaction make permeability measurement gas dependent. For highly heterogenous macroscopic pores or fractures of unconventional reservoirs, permeability measurement with nitrogen or mercury is not appropriate for the performance evaluation of a natural gas reservoir. The use of the main gas component (Methane) to measure permeability is better and reliable estimation approach.

Brace et al. (1968) first derived the equation that calculates permeability by ignoring the compressibility storage effect. Jia et al. (2018) established the heterogeneity effect's contribution that influences flow behavior based on the complexity between adsorption and permeability, as shown in

Simulated pressure means the endmost equilibrium pressure for each pressure step and typifies similar pressure to determine permeability.

pulse decay experiments of three different gases. Kamath et al. (1992) infused two dissimilar cores longitudinally of different permeability with the inflow of water in forward and reverse directions. The results showed that pressure responses are direction-dependent, which affirmed that heterogeneity is a critical parameter in the pulse decay experiment.

The assumptions used in Cui et al. (2009) experimental work of late time data is that gas properties are constant, although making such assumption generate significant errors. Pressure dependent intrinsic properties are of greater relevance in estimating and measuring the permeability of ultra-low permeability rocks.

2.7.1 Advantages of Pulse Decay/ Unsteady Technique over Conventional Methods of Permeability

1. Non-sophisticated equipment is required.
2. It has easy operational procedures.
3. Measurement of permeability is easy.
4. Measurement is reliable and fast because the lessening time varies with the square of the sample radius.
5. Higher reliability, unlike the conventional approach.
6. The inclusion of the compressive storage and sorption effects eliminates errors in permeability measurement.

Simulated pressure means the endmost equilibrium pressure for each pressure step and typifies similar pressure to determine permeability.

Chapter Three

3.1 Experimental Layout

Before the experiment, the rock samples were shortened to about 2 inches with a diameter of 1 inch. A drying procedure was done for 24 hours and then put into aluminum foil (prevents interaction between sample and rubber jacket) placed in a rubber jacket (it prevents contact of the sample with confining gas). The experimental set-up replicates Wang et al. (2015), with various valves ranging from 1 to 4. Gas flow into the sample is controlled by valve 1. The gas flow into the downstream reservoir is controlled by valve 2, while valves 3 and 4 controlled confining stress and axial load on the specimen from the triaxial cell.

The gas cylinder is embedded symmetrically with the two reservoirs on the left-hand side of the triaxial cell. The gas cylinder gives additional pressure to compensate for pressure in the upstream reservoir. The pressure pulsation is measured at the upstream and downstream reservoirs by two installed pressure transducers. Temperature is constant during the experiment, and the permeability is measured based on the pressure variations.

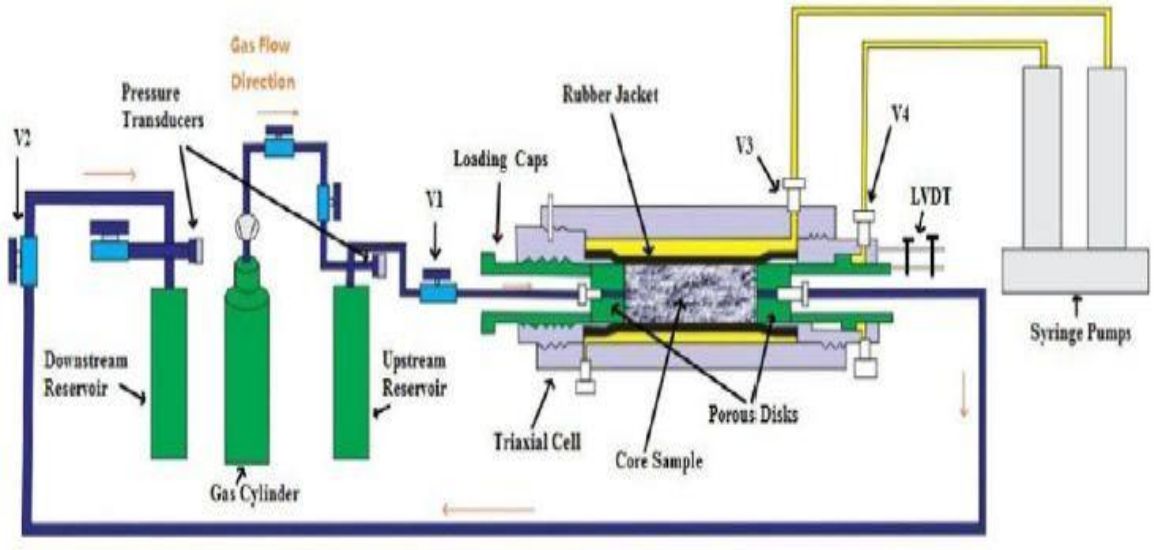

Figure 4: Experimental Setup (Wang et al. *(2015)*)

3.2 Experimental Approach

The subsequent injection of three gases, namely methane, carbon dioxide, and helium, was used to study permeability measured at steady stress boundary conditions. The first cycle injection used helium, which is a non-sorbent gas. The helium gas was injected at a pressure of $14\ psi$ into the upstream and downstream reservoirs until established in the downstream reservoir. However, the upstream had a continuous injection of helium gas until $31\ psi$. The gas injection introduction is by increasing the confining stress steadily to $1000\ psi$ and a steady increase of axial load to $696\ psi$. The pressure of $31\ psi$ in the upstream constituted the enabling force for the gas flow. The reservoir's

Simulated pressure means the endmost equilibrium pressure for each pressure step and typifies similar pressure to determine permeability.

confinement prevents interaction with downstream and triaxial cell by opening valve 1, which permits gas flow into the specimen. When the equilibrium is established in the system, the experiment ends. From the pressure pulsation, the estimation of permeability occurred. A cyclic pattern established as the initial pressure ended. Values of pressures at upstream and downstream increased until equilibrium. The process involves six different pressure injection with helium. The same cyclic procedure is performed for methane and carbon dioxide for permeability measurements at the same confining and axial stresses.

3. 3 Mathematical Model Development

The model's development is from the governing equation with assumptions that intrinsic gas properties are pressure-dependent based on the experimental set-up of Wang et al. (2015). The governing equation comprises gas compressibility storage effect, gas desorption or adsorption, and gas slippage effect. The comprehensive form model gives a non-linear equation that is solved by a numerical scheme of the finite difference approach. The model simulation is with MATLAB.

3. 4 Methodology

3. 4. 1 Model Assumptions

- Porosity is constant in time.
- Single gas-phase flow.
- One dimensional linear flow.
- Isothermal flow condition is present through the experiment.
- Pressure dependent gas density.
- Gas viscosity is constant.
- Gas adsorption-desorption kinetics conforms with the Langmuir curve, which implies equilibrium for any reservoir pressure.

3. 4. 2 Model Development

The mass conservation equation from the general form is.

$$\phi \frac{\partial \rho}{\partial t} = \frac{\partial}{\partial x}(\rho\, u\,) \tag{21}$$

Introduce adsorption term to the RHS of equation (15)

$$\phi \frac{\partial \rho}{\partial t} + (1-\phi)\frac{\partial C}{\partial t} = \frac{\partial}{\partial x}(\rho\, u\,) \tag{22}$$

Where ϕ is porosity, ρ is gas density, C is the density adsorption per unit density of the rock.

Darcy Equation

$$u = -\frac{k}{\mu}\frac{\partial p}{\partial x} \tag{23}$$

Simulated pressure means the endmost equilibrium pressure for each pressure step and typifies similar pressure to determine permeability.

Adsorption

Adsorption of the gas expression for gas volume per unit bulk volume of unconventional rock is.

$$C = \frac{\rho_s C_e}{V_{std}} \quad (24)$$

The expression for Volume of the gas adsorbed is:

$$C_e = \frac{q_L P}{P + P_L} \quad (25)$$

Put equation (19) into equation (18)

$$C = \frac{\rho_s}{V_{std}} \frac{q_L P}{P+P_L} \quad (26)$$

C is adsorption density per unit unconventional reservoir volume, q_L is Langmuir gas volume, C_e is adsorbed gas volume, $_{P.L}$. is the pressure of Langmuir, V_{std} is the Volume of the sample under investigation.

Basic Gas Equation

The gas density is determined by,

$$\rho = \frac{P}{ZRT} \quad (27)$$

Gas Compressibility

The gas compressibility expressed at isothermal temperature is:

$$C_g = \frac{1}{\rho}\left(\frac{\partial \rho}{\partial P}\right)_{.T.} \quad (28)$$

Re-arrange equation (22),

$$\rho\, C_g = \left(\frac{\partial \rho}{\partial P}\right)_T \quad (29)$$

An expression for the time derivative of accumulation is:

$$\frac{\partial \rho}{\partial t} = \frac{\partial \rho}{\partial P} \frac{\partial P}{\partial t} \quad (30)$$

Simulated pressure means the endmost equilibrium pressure for each pressure step and typifies similar pressure to determine permeability.

Insert equation (17) into equation (16).

The complete model equation is given below, which is a non-linear variable because the gas properties are varying.

$$\phi \frac{\partial \rho}{\partial t} + (1-\phi)\frac{\partial C}{\partial t} = \frac{\partial}{\partial x}\left(\frac{k\rho}{\mu}\frac{\partial P}{\partial x}\right) \tag{31}$$

Initial Condition

The initial condition is explicitly expressed as the pressure at the downstream at the initial condition.

$$P(x, t=0) = P_d \qquad for\ range\ 0 < r < L \tag{32}$$

Boundary Condition

For boundary conditions, all equations depend on mass balance, and the change of the gas amount is equivalent to the amount of gas inflow or outflow.

In the upstream

$$P(x=0, t) = P_u \qquad for\ any\ time\ t \geq 0 \tag{33}$$

At the downstream

$$P(x=L, t) = P_d \qquad for\ any\ time\ t \geq 0 \tag{34}$$

Develop mass conservation equations upstream and downstream.

$$\frac{\rho K A}{\mu}\frac{dP}{dx}|_{r=0} = V_u \frac{d\rho_u}{dt} \qquad for\ any\ time\ t > 0 \tag{35}$$

$$\frac{\rho K A}{\mu}\frac{dP}{dx}|_{r=L} = V_d \frac{d\rho_d}{dt} \qquad for\ any\ time\ t > 0 \tag{36}$$

Numerical Simulation

$$\phi \frac{\partial \rho}{\partial t} + (1-\phi)\frac{\partial C}{\partial t} = \frac{\partial}{\partial x}\left(\frac{k\rho}{\mu}\frac{\partial P}{\partial x}\right) \tag{37}$$

Insert equation (21) into equation (31)

$$\frac{\phi}{RT}\frac{\partial\left(\frac{P}{Z}\right)}{\partial t} + (1-\phi)\frac{\partial C}{\partial t} = \frac{\partial}{\partial x}\left(\frac{k\rho}{\mu}\frac{\partial P}{\partial x}\right) \tag{38}$$

Simulated pressure means the endmost equilibrium pressure for each pressure step and typifies similar pressure to determine permeability.

The numerical solution for the general model equation is given in equation (32):

$$\frac{\phi}{RT}\frac{\left(\frac{P_i^{(r+1)}}{Z_i^{(r)}}\right)^{n+1}-\left(\frac{P}{Z}\right)_i^n}{\Delta t}+(1-\phi)\frac{C_i^{n+1\ (r)}-C_i^n}{\Delta t}$$
$$=\left(\frac{k\rho}{\mu\Delta x^2}\right)_{i+\frac{1}{2}}^{n+1^{(r)}} P_{i+1}^{n+1^{(r+1)}}$$
$$-\left[\left(\frac{k\rho}{\mu\Delta x^2}\right)_{i+\frac{1}{2}}^{n+1^{(r)}}+\left(\frac{k\rho}{\mu\Delta x^2}\right)_{i-\frac{1}{2}}^{n+1^{(r)}}\right] P_i^{n+1\ (r+1)} \tag{39}$$
$$+\left(\frac{k\rho}{\mu\Delta x^2}\right)_{i-\frac{1}{2}}^{n+1^{(r)}} P_{i-1}^{n+1\ (r+1)}$$

The iteration step represents by r. Implementation of average harmonic estimation for the middle term in RHS of equation (33)

$$\left(\frac{k\rho}{\mu\Delta x^2}\right)_{i+\frac{1}{2}}=\frac{1}{\left(\frac{k\rho}{\mu\Delta x^2}\right)_{i+\frac{1}{2}}}=\frac{1}{2}\left[\frac{1}{\left(\frac{k\rho}{\mu\Delta x^2}\right)_i}+\frac{1}{\left(\frac{k\rho}{\mu\Delta x^2}\right)_{i+1}}\right] \tag{40}$$

$$\left(\frac{k\rho}{\mu\Delta x^2}\right)_{i-\frac{1}{2}}=\frac{1}{\left(\frac{k\rho}{\mu\Delta x^2}\right)_{i-\frac{1}{2}}}=\frac{1}{2}\left[\frac{1}{\left(\frac{k\rho}{\mu\Delta x^2}\right)_i}+\frac{1}{\left(\frac{k\rho}{\mu\Delta x^2}\right)_{i-1}}\right] \tag{41}$$

The numerical expression above is for $1 \leq i \leq N_x$. The number grid block is represented by N_x, which does not include the boundary grid block. The old-time level and new time level are denoted by N and $N+1$, respectively. i denotes the centre of the grid block. The upstream location is represented by $i=1, i-1$, while the downstream location is $i=N_x, i+1$. Space and time steps are denoted respectively by Δx and Δt in the numerical simulation.

The Δx from this expression is:

$$\Delta x = \frac{L}{N_x+1} \tag{42}$$

From equation (36), L is the length of the sample (Grid block boundary from the left end to grid block boundary at the right end). The distance between the grid block centre to centre is equal, therefore:

$$\Delta x = \Delta_{x1} = \Delta_{x1} = \Delta_{x1} = \cdots = \Delta x_{N_x} = \frac{L}{N_x+1} \tag{43}$$

Simulated pressure means the endmost equilibrium pressure for each pressure step and typifies similar pressure to determine permeability.

The values of upstream and downstream pressures at new time steps would be the inputs calculated from the numerical solution of the boundary conditions.

$$\frac{\rho\, KA}{\mu}\,\frac{P(1)^n - P_u^n}{\Delta x} = V_u\,\frac{\rho\,{}_u^{n+1} - \rho\,{}_u^{n}}{\Delta t} \tag{44}$$

$$\frac{\rho\, KA}{\mu}\,\frac{P(N_x)^n - P_d^n}{\Delta x} = V_d\,\frac{\rho\,{}_d^{n+1} - \rho\,{}_d^{n}}{\Delta t} \tag{45}$$

3.5 Constant Gas Properties Approach

By making some modifications to the above model such that varying gas properties are kept constant, the general model for constant gas properties becomes (Cui et al.,2009):

$$\frac{\partial \rho}{\partial t} = \frac{k}{\mu C_g(\phi + (1-\phi\,)k_a)}\frac{\partial^2 P}{\partial x^2} \quad for\ 0 < x < L, \qquad at\ \ t > 0 \tag{46}$$

The above equation estimate pressure as it varies along with the cylindrical sample.

The initial condition gives:

$$P(r, t = 0) = P_d \qquad for\ range\ 0 < r < L \tag{47}$$

The Boundary conditions for the constant gas properties modelling are below.

$$P(r = 0, t) = P_u\ (t) \qquad for\ any\ time\ t \geq 0 \tag{48}$$

$$P(r = L, t) = P_d\ (t) \qquad for\ any\ time\ t \geq 0 \tag{49}$$

Mass conservation development based on the initial and boundary condition for the upstream and downstream are as follows:

$$\frac{KA}{\mu}\frac{dP}{dx}|_{r=0} = V_u\,\frac{d\rho_u}{dt} \qquad for\ any\ time\ t > 0 \tag{50}$$

$$\frac{KA}{\mu}\frac{dP}{dx}|_{r=L} = V_d\,\frac{d\rho_d}{dt} \qquad for\ any\ time\ t > 0 \tag{51}$$

Simulated pressure means the endmost equilibrium pressure for each pressure step and typifies similar pressure to determine permeability.

3.7 Model History Matching Approach

The upstream and downstream pressures are calculated at the next time step for density conversion to pressure. Assume an initial guess of pressure distribution along the specimen P. For simplicity, it is equal to the pressure distribution at the previous time step. Solve for the pressure distribution and the specimen at the next iteration: update time step, the pressure distribution of the entire system, and the corresponding gas properties. The new simulated pressures matched with the experimental pressures.

The numerically simulated outcomes with varying permeability indicate that the rate of pressure difference is affected by high and low permeabilities of varying and constant conditional pressure gas properties. The rate of pressure decline decreases with low permeability and vice versa for high permeability. It is evident from Figure 6 that low permeability causes pressure to increase; hence gas accumulates. In contrast, high permeability causes a reduction in the quantity of gas in the reservoir at a higher pressure reduction rate. Since permeability influences the shape of the pressure outline, it is important to history-match the outcomes of experimental and simulated pressures. The difference in values of simulated and experimental pressure outcomes can be described and assess from the equation below. The equation below refers to an objective function that determines the disparity in pressure measurement from the upstream and downstream of experimental and simulated values. The quality of the history matched pressures is checked based on the equation (51).

$$R = \frac{\sum_{i=1}^{S}\left(\left|\frac{P_{Sim_i} - P_{Exp_i}}{P_{Exp_i}}\right|\right)_{upstream} - \sum_{i=1}^{S}\left(\left|\frac{P_{Sim_j} - P_{Exp_j}}{P_{Exp_j}}\right|\right)_{downstream}}{S + H} X\ 100\% \qquad (52)$$

P_{Sim} and P_{Exp} are simulated and experimental pressure, S and H are data points, and i, j are time steps. The objective function permeability converges towards optimization based on the set tolerance of 0.025.

Figure 5 shows an example of history matched simulated pressure for different pressure steps, and the corresponding permeability for both upstream and downstream reservoirs.

Simulated pressure means the endmost equilibrium pressure for each pressure step and typifies similar pressure to determine permeability.

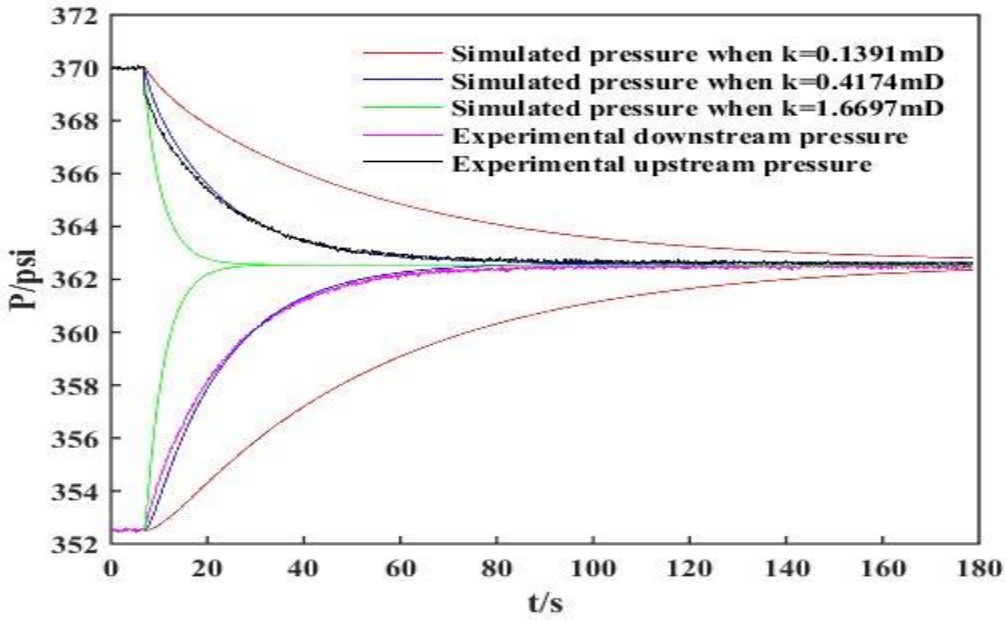

Figure 5: History Match of simulated pressure with varying permeabilities and experimental downstream and upstream pressures.

Simulated pressure means the endmost equilibrium pressure for each pressure step and typifies similar pressure to determine permeability.

Chapter 4

Result and Discussion

Analysis of the sample permeability occurred using Carbon dioxide, Helium, and Methane. These gases have properties that are suitable for this study. Carbon dioxide and methane have sorption properties, unlike helium. The sorption and varying gas properties are instrumental in the sensitivity analysis of the model. The comparison of this method shows a better outcome than that of Cui et al. (2009). The simulated pressure and the corresponding permeability are the unknowns. The experimental data used in this study is from the Department of Petroleum Resources. The plots of the results in section 4.1 were generated based on equation (38).

4.1 Results Presentation

4.1.1 Flushing Carbon dioxide through the sample

The adsorptive characteristics of carbon dioxide are higher relative to its high Langmuir volume and low Langmuir pressure. This characteristic of carbon dioxide is a distinctive feature against methane and helium gases. The excellent adsorptive characteristics of carbon dioxide account for a higher-pressure reduction rate after the stabilization of pressure. Table 2 shows the data used to estimate carbon dioxide to determine the pressure decay of permeability.

Table 1: Variables inputs used for Carbon dioxide.

Variable	Step					
	1	2	3	4	5	6
P_{ui} *(psi)*	32.20	118.64	231.85	348.23	476.88	592.30
P_{di} *(psi)*	14.70	101.15	214.85	330.48	459.31	574.93
μ *(Pa*s)*	0.00001484	0.00001490	0.00001501	0.00001519	0.00001548	0.00001588
C_g (Psi^{-1})	0.0460	0.00955	0.00491	0.00344	0.00273	0.00245
V_u (m^3)	0.00002998	0.00002998	0.00002998	0.00002998	0.00002998	0.00002998
$V_d(m^3)$	0.0000178	0.0000178	0.0000178	0.0000178	0.0000178	0.0000178
L (m)	0.0602	0.0602	0.0602	0.0602	0.0602	0.0602
A (m^2)	0.000507	0.000507	0.000507	0.000507	0.000507	0.000507
ϕ	0.12	0.12	0.12	0.12	0.12	0.12
P_e *(psi)*	21.90	109.12	223.35	339.52	468.46	584.19
q_L*(scf/ton)*	1170	1170	1170	1170	1170	1170
P_L *(psi)*	287.41	287.41	287.41	287.41	287.41	287.41

Data used is from the Department of Petroleum Resources, Nigeria

Figure 7 shows the Carbon Dioxide history match of the simulation and experimental for upstream and downstream. Table 3 shows a summary of the outcomes of permeability. It is evident that permeability declines at the beginning with a steady recovery later, for increasing pressure rate. Although, this trend explains the large adsorption of carbon dioxide with a swelling effect in the matrix. The swelling

Simulated pressure means the endmost equilibrium pressure for each pressure step and typifies similar pressure to determine permeability.

impacted permeability reduction because the amount of carbon dioxide adsorbed has reduced with the increasing pressure of Langmuir sorption characteristics.

Table 2: Estimated Permeability based on pressure values of carbon Dioxide.

Step	Pressure(psi)	Permeability (mD)	Objective function R (%)
1	21.900	1.480	2.400
2	109.120	0.900	0.380
3	223.350	0.620	0.210
4	339.520	0.550	0.120
5	468.400	0.590	0.069
6	584.190	0.660	0.045

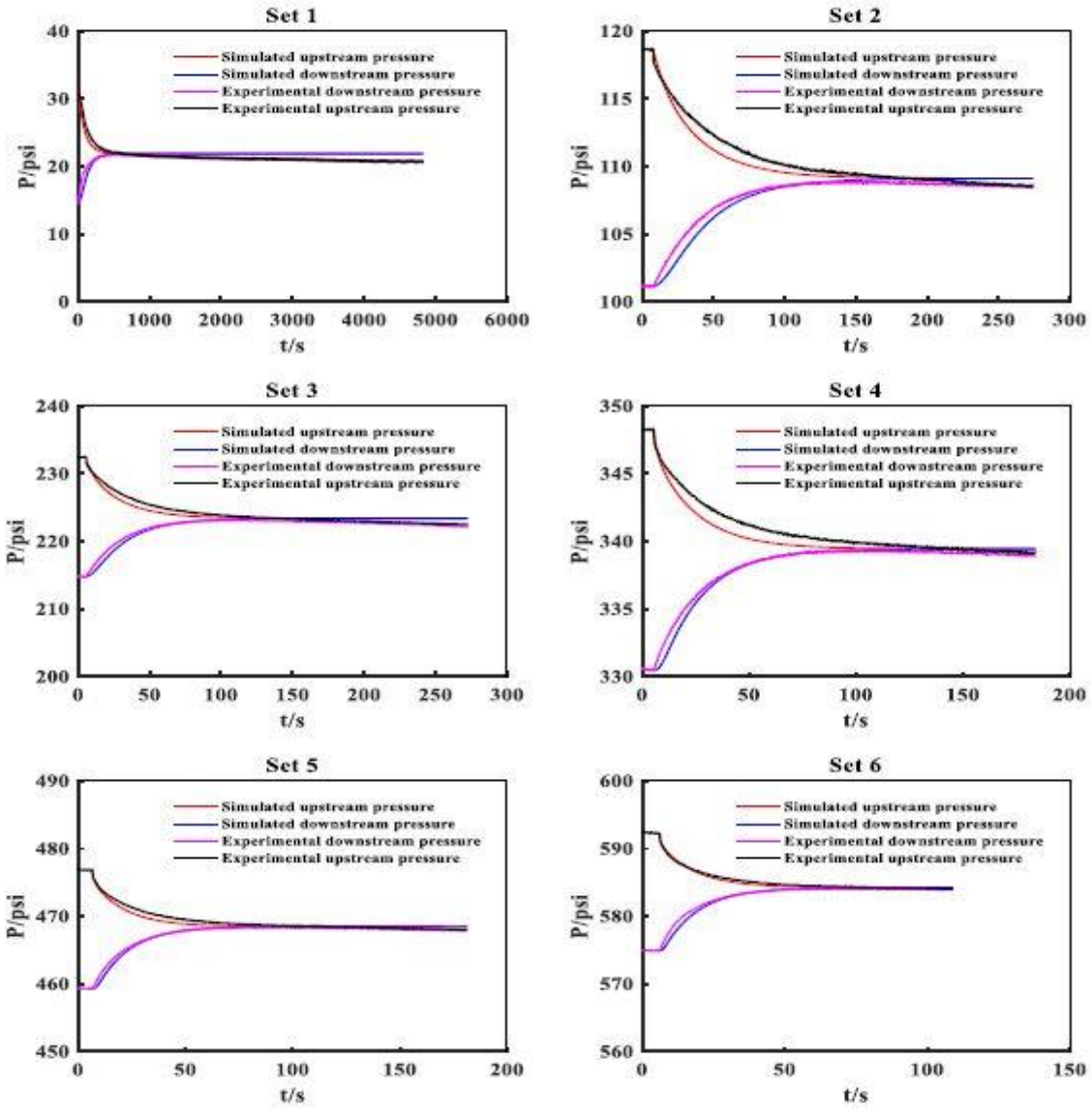

Figure 6: Carbon Dioxide History Match of Simulation, Experimental for upstream and downstream.

Simulated pressure means the endmost equilibrium pressure for each pressure step and typifies similar pressure to determine permeability.

4.1.2 Flushing Methane through Sample

The simulated output of methane is presented from the inputs in Table 4. Adsorption is relevant to gas storage in the reservoir matrix—the impact of Langmuir parameters needed investigation for better understanding.

Table 3: Variables inputs used for methane.

Variable	Step					
	1	2	3	4	5	6
P_{ui} *(psi)*	32.05	141.79	256.51	370.05	482.65	610.04
P_{di} *(psi)*	14.71	124.29	238.92	352.54	464.96	592.59
μ *(Pa*s)*	0.00001102	0.00001113	0.00001125	0.00001139	0.00001155	0.00001175
C_g (Psi^{-1})	0.0424	0.00759	0.00415	0.00288	0.00223	0.00178
V_u (m^3)	0.00002998	0.00002998	0.00002998	0.00002998	0.00002998	0.00002998
$V_d(m^3)$	0.0000178	0.0000178	0.0000178	0.0000178	0.0000178	0.0000178
L (m)	0.0602	0.0602	0.0602	0.0602	0.0602	0.0602
A (m^2)	0.000507	0.000507	0.000507	0.000507	0.000507	0.000507
ϕ	0.12	0.12	0.12	0.12	0.12	0.12
P_e *(psi)*	23.64	133.87	248.59	362.58	474.98	602.45
q_L*(scf/ton)*	393.3	393.3	393.3	393.3	393.3	393.3
P_L *(psi)*	380.24	380.24	380.24	380.24	380.24	380.24

Data used is from Department of Petroleum Resources, Nigeria.

Figure 8 shows the set of history matched outcomes for methane gas flushing on the sample. The sample's storage capacity increased because of pressure reduction that occurred after the establishment of pressure equilibrium between pressures upstream and downstream (Aljamaan, 2013). Equation 25 is not affected by the established equilibrium of pressure from the history matched profile. Therefore, permeability estimation is based on excluding the equilibrium pressure in the pressure profile, which reduces the time for estimating permeability. In other words, the time required for the estimation of permeability reduces as the time for the establishment of equilibrium is not considered.

From table 5, the permeability estimation is based on the pressure with objective function for methane on the sample. Pressure increases from step 1 to step 6 at a range of $23.640\ psi$ to $602.400\ psi$, which initially increased permeability at $23.640\ mD$ to $0.870\ mD$. The progressive increment is related to impacts of sorption, swelling of matrix mechanisms. From this simulation, it is evident that permeability increases are dependent on pressure increases. However, changes in permeability are primarily impacted by pressure. Therefore, the sorption effect causes matrix swelling with minimal impact.

Simulated pressure means the endmost equilibrium pressure for each pressure step and typifies similar pressure to determine permeability.

Table 4: Estimated Permeability based on pressure values of methane.

Step	Pressure(psi)	Permeability (mD)	Objective function R (%)
1	23.640	0.250	1.900
2	133.870	0.310	0.260
3	248.590	0.360	0.098
4	362.580	0.420	0.030
5	474.980	0.540	0.026
6	602.410	0.870	0.022

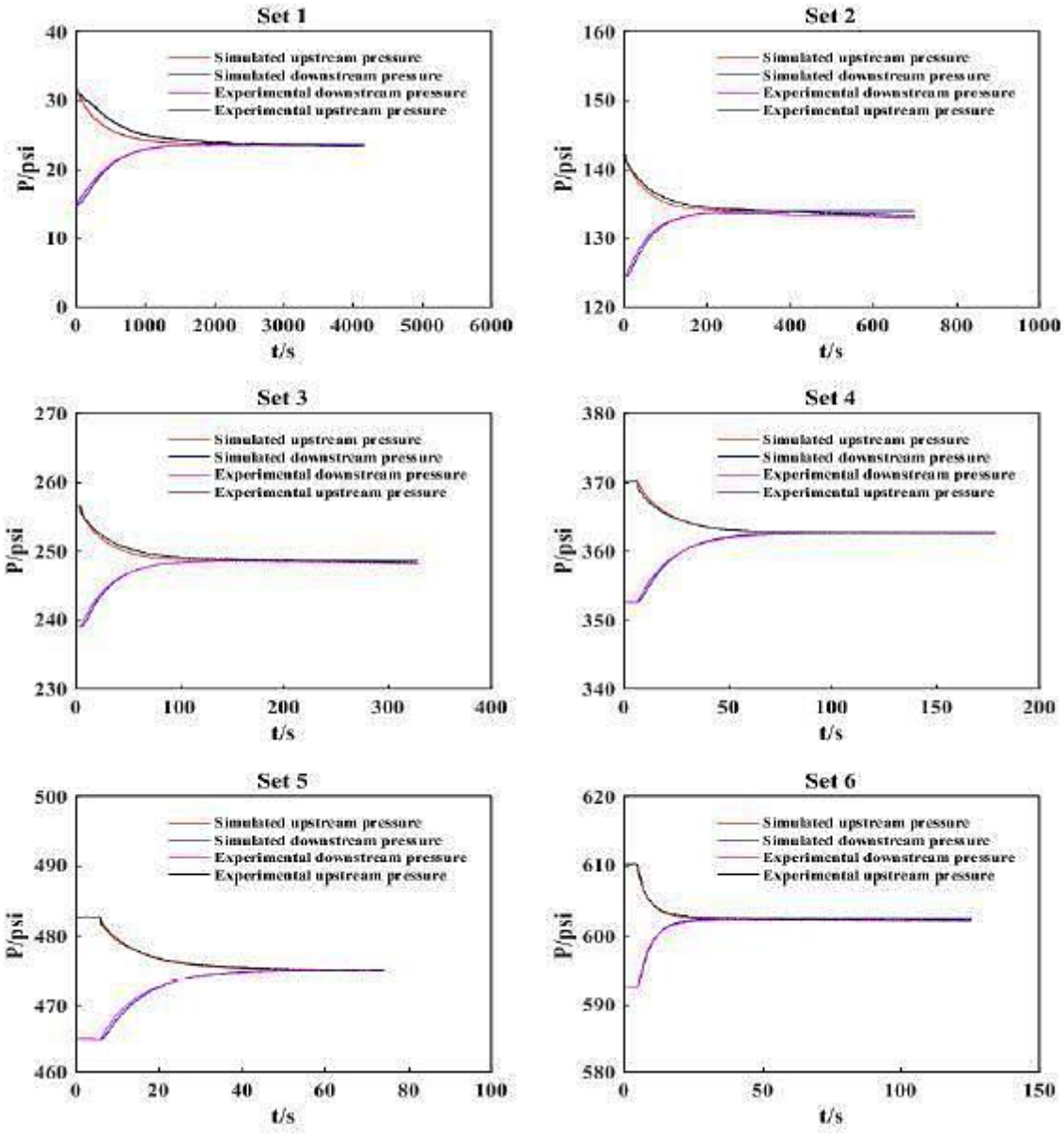

Figure 7: Methane History Match of Simulation, Experimental for upstream, and downstream.

4.1.3 Flushing Helium through Sample

The estimation of permeability with helium flushing on the sample, as shown in Table 6. The pressure at which permeability estimation occurs is the stabilization pressure.

Simulated pressure means the endmost equilibrium pressure for each pressure step and typifies similar pressure to determine permeability.

Table 5: Variables inputs used for helium.

Variable	Step					
	1	2	3	4	5	6
P_{ui} *(psi)*	31.33	148.13	264.25	380.33	496.43	613.38
P_{di} *(psi)*	14.71	130.48	246.72	363.15	478.51	595.35
μ *(Pa*s)*	0.00001976	0.00001979	0.00001981	0.00001984	0.00001987	0.00001990
C_g (Psi^{-1})	0.0408	0.00708	0.00386	0.00265	0.00201	0.00162
V_u (m^3)	0.00002998	0.00002998	0.00002998	0.00002998	0.00002998	0.00002998
$V_d(m^3)$	0.0000178	0.0000178	0.0000178	0.0000178	0.0000178	0.0000178
L (m)	0.0602	0.0602	0.0602	0.0602	0.0602	0.0602
A (m^2)	0.000507	0.000507	0.000507	0.000507	0.000507	0.000507
ϕ	0.12	0.12	0.12	0.12	0.12	0.12
P_e *(psi)*	24.51	140.54	256.75	372.89	488.69	605.47

Data used is from the Department of Petroleum Resources, Nigeria.

Figure 9 depicts the history approximate of simulated outputs. The plots showed a consistent reproduce of experimental data plots, as seen in Table 7. The tolerance of the objective function is not exceeded. The distinctive characteristic of helium is its lack of sorption impacts, which results in increased permeability as a function of increased pressure. The pressure increases at a range of $24.510\ psi$ to $605.470\ Psi$ for a corresponding increase in permeability at range $0.870\ mD$ to $2.910\ mD$.

Table 6: Estimated Permeability based on pressure values of helium.

Step	Pressure(psi)	Permeability (mD)	Objective function R (%)
1	24.510	0.870	0.480
2	140.540	0.820	0.037
3	256.750	0.980	0.020
4	372.890	1.240	0.022
5	488.690	1.650	0.014
6	605.470	2.910	0.011

Simulated pressure means the endmost equilibrium pressure for each pressure step and typifies similar pressure to determine permeability.

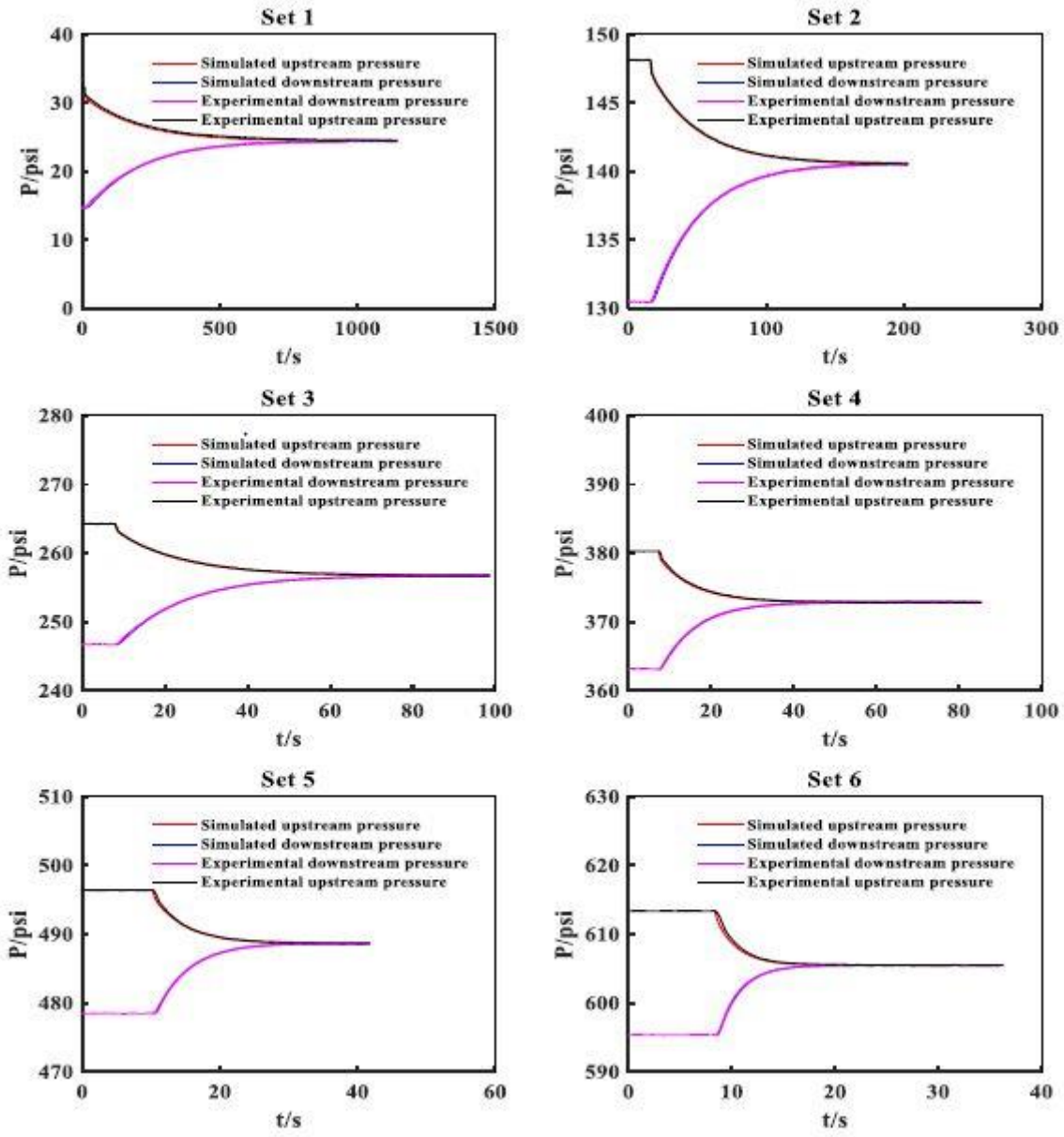

Figure 8: Helium History Match of Simulation, Experimental for upstream, and downstream.

4.1.4 Variance in Permeability with Selected Gases

From tables 3, 5, and 7, the variation in the permeabilities of carbon dioxide, Helium, and Methane as depicted by the plot of gases permeabilities versus pressure in Figure 10. It is evident that at a pressure of above $150\ psi$, helium has the highest permeability. The highest value of helium permeability distinguishes it from other studied gases as helium has negligible sorption effect, a least molecular diameter that enables accessibility of minute pores, and significant gas slippage effect. The sorption effect is dominant in carbon dioxide as permeability decreases above $200psi$.

Simulated pressure means the endmost equilibrium pressure for each pressure step and typifies similar pressure to determine permeability.

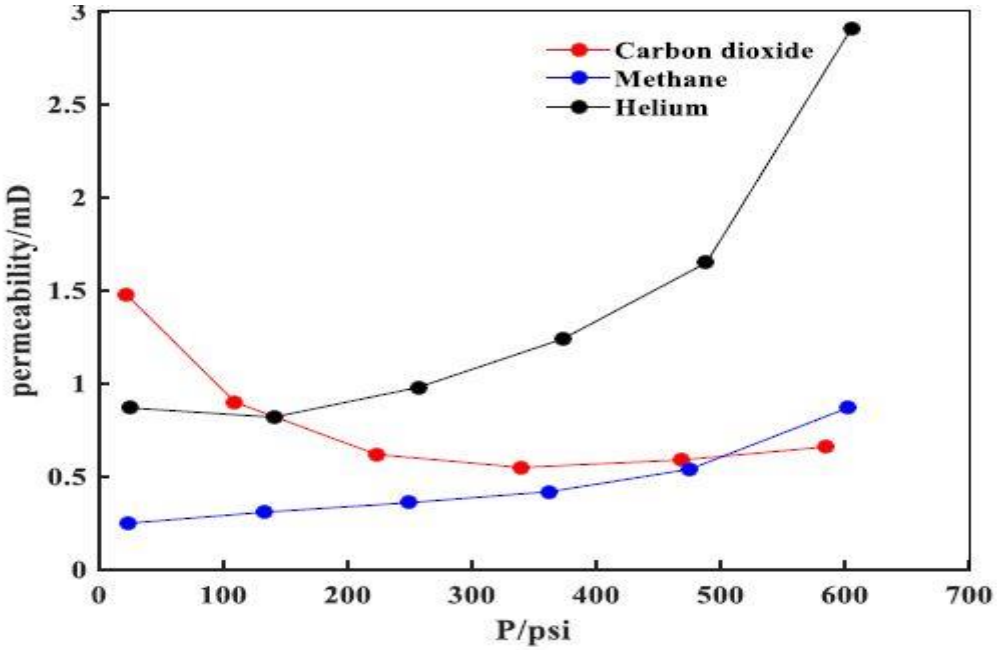

Figure 9: Comparative permeability plots of studied gases as a function of pore pressure.

4.2 Sensitivity Analysis

A methodical approach to investigating intrinsic factors influencing the estimation of estimation. This study's approach centred on varying or constant gas properties as against the analytical approach of Cui et al. (2009) to simulate history matching. Different permeability approaches were evaluated and compared based on their effects on estimated permeability. The study of the systematic investigation of intrinsic factors' influence on permeability estimation is for better understanding.

4.2.1 Results Evaluation of Permeability based on various Models.

The three studied methods used in estimating the different gases' permeability under investigation and the results are comparatively weighed. The analytical solution approach from equation (15), termed an analytical solution. The numerical simulation based on equation (38), for varying gas properties approach, is called numerical solution 1, while the numerical solution with constant gas properties from equation (46) is called numerical solution 2.

Table 7: Numerical and Analytical solutions for Helium Flushed Sample for determining permeability.

Step	Pressure(psi)	Analytical solution (mD)	Numerical solution 2 (mD)
1	24.51	0.72	0.82
2	140.54	0.84	0.82
3	256.75	1.00	0.97
4	372.89	1.28	1.23
5	488.69	1.80	1.62
6	605.47	3.02	2.87

Simulated pressure means the endmost equilibrium pressure for each pressure step and typifies similar pressure to determine permeability.

Table 8: Numerical and Analytical solutions for Methane Flushed Sample for determining permeability.

Step	Pressure(psi)	Analytical solution (mD)	Numerical solution 2 (mD)
1	23.64	0.19	0.24
2	133.87	0.28	0.3
3	248.59	0.31	0.36
4	362.58	0.42	0.41
5	474.98	0.45	0.53
6	602.45	0.62	0.85

Table 9: Numerical and Analytical solutions for Carbon Dioxide Flushed Sample for determining Permeability.

Step	Pressure(psi)	Analytical solution (mD)	Numerical solution 2 (mD)
1	21.9	1.75	1.43
2	109.12	0.88	0.89
3	223.35	0.54	0.62
4	339.52	0.38	0.55
5	468.46	0.41	0.58
6	584.19	0.47	0.66

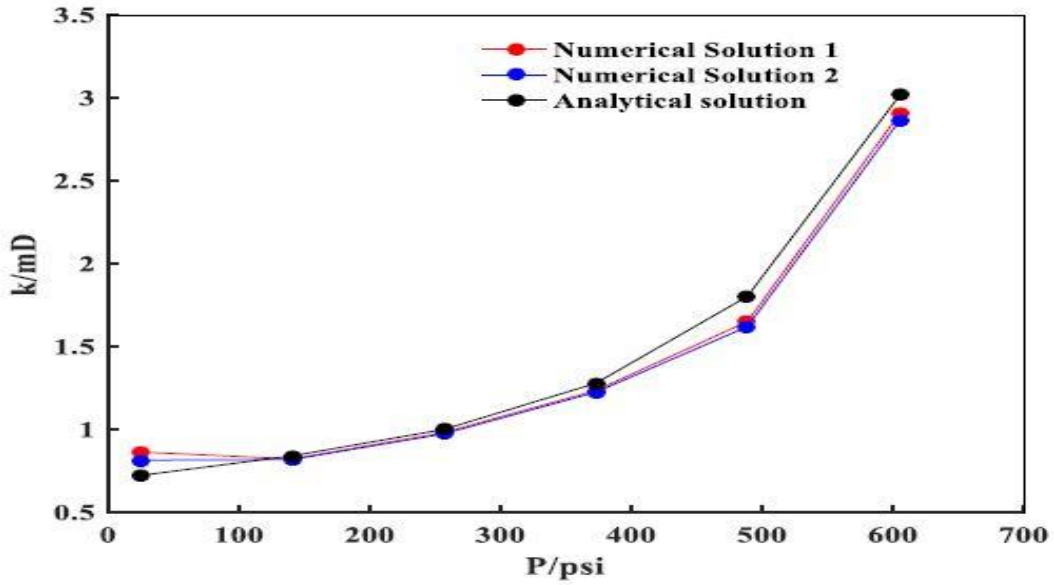

Figure 10: Plot of permeability versus pressure for helium to compare various methods of permeability estimation.

Simulated pressure means the endmost equilibrium pressure for each pressure step and typifies similar pressure to determine permeability.

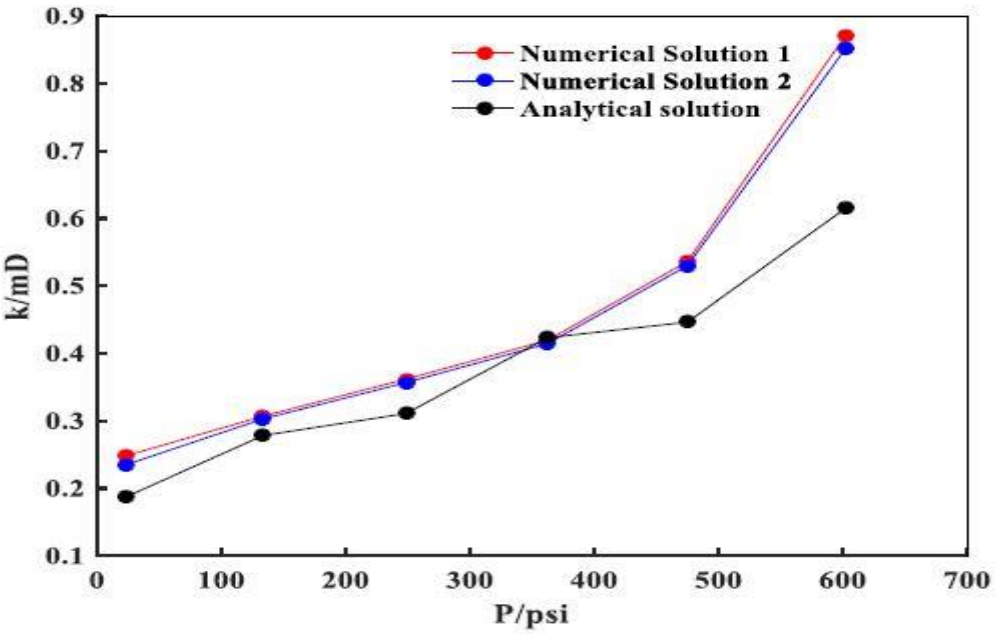

Figure 11: Plot of permeability versus pressure for methane to compare various methods of permeability estimation.

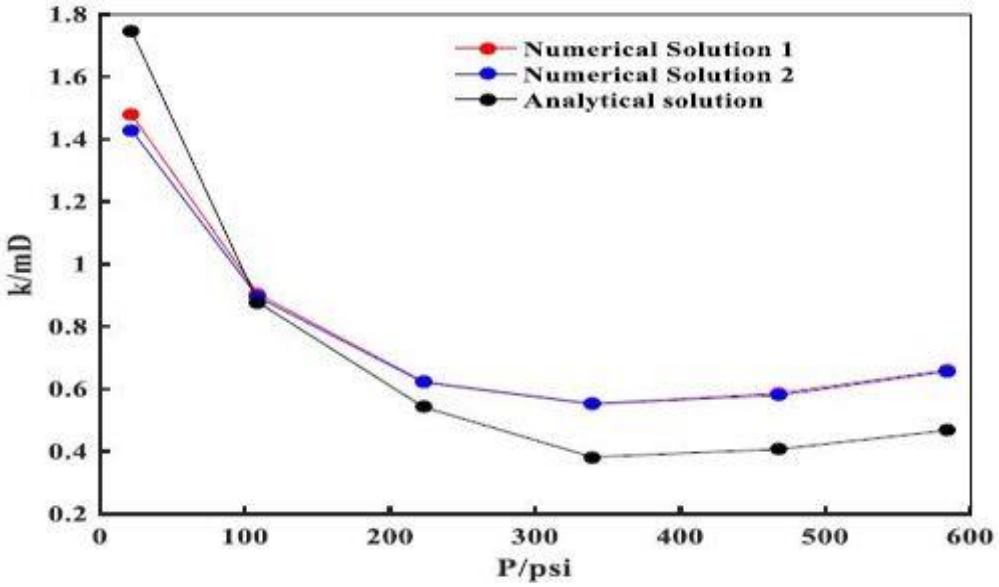

Figure 12: Plot of permeability versus pressure for carbon dioxide to compare various methods of permeability estimation.

Figures 10 to 12 show comparative graphical representation of analytical solution and numerical solution 2 for the adsorptive gases under study, using data from Tables 8 to 10. From the graphs, it is evident that the disparity in analytical solution values and numerical solution 1 is subject to two reasons.

Simulated pressure means the endmost equilibrium pressure for each pressure step and typifies similar pressure to determine permeability.

1. From the assumption that constant gas properties are pressure-dependent, the lower initial pressure or considerable differential pressure along the sample caused a notable error for the analytical solution. From figures 11 to 13, the numerical solutions 1 and 2 are approximately equal for high initial core pressure. A non-consistent permeability difference occurs for lower initial core pressure, although there is no effect on permeability outcome.

for little pressure difference.

2. The numerical solution of permeability, estimation centred on the outline simulated and experimental pressures, and an analytical solution as determined from the late-time slope of pressure match. The relative error impacted by either varied or constant gas properties is lesser than that of relative errors from the pressure match for the three gases. Therefore, the impact on permeability outcome occurs through the variation of experimental pressure data and simulated trends. Simulated and experimental pressure outlines best fit cannot by mere matching late-time slopes alone. Convolution of flow mechanisms in adsorptive gases exhibits higher relative error than gas without the adsorptive feature (Helium) for varied gas properties.

From the two established reasons above, it is evident that the second reason significantly influenced the permeability results estimation. Permeability estimation is realistic with a history matching approach. A systematic approach uses varying gas properties at the initial pressure step but applying constant gas properties give more accurate results as pressure increases.

4.3 Sensitivity of Differential Pressure to Porosity

Using values from Table 2 with a constant permeability of $0.66\ mD$, and varying values of porosity in succession of $0.001, 0.01, 0.05, 0.08, 0.12, \text{and } 0.15$. Figure 14 shows pressure plots for varying porosities. Varying porosity cannot influence permeability estimation outcomes based on experimental pressure difference outcomes. This assertion negates the work of Bergs (1970) relative to the established permeability-porosity dependency. As porosity declines from the highest selected porosity value of 0.15 to the lowest value 0.001, this should cause a significant decrease in permeability. Therefore, different samples of different porosities will yield different results for differential pressure, then permeability estimation varies.

Simulated pressure means the endmost equilibrium pressure for each pressure step and typifies similar pressure to determine permeability.

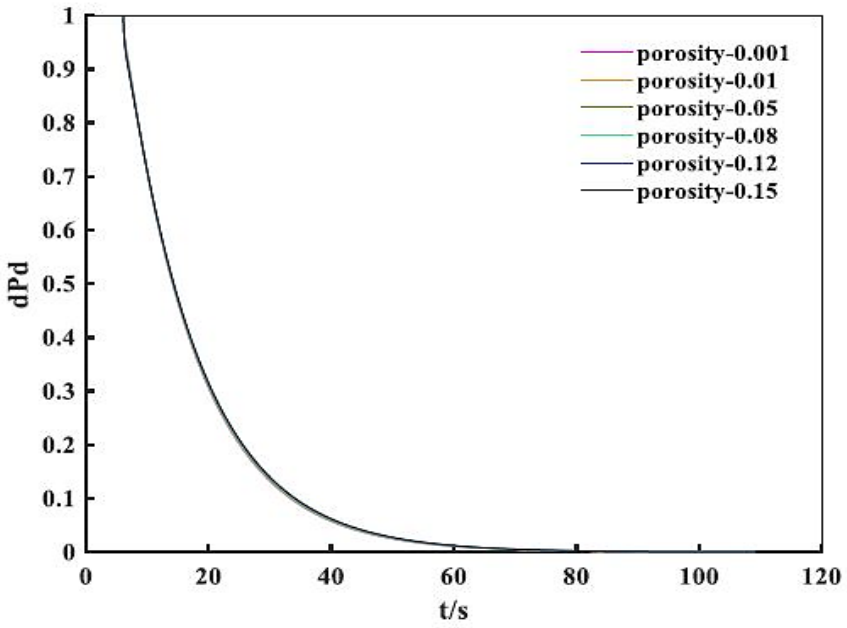

Figure 13: Plot of differential pressure versus time for varying porosity values

4.4 Sensitivity of Differential Pressure to Gas Compressibility

The differential pressure for various gases with reference to varying gas compressibility. The highest gas compressibility shows a significant effect on the permeability. This effect is prevalent even with a small pressure difference, and gas compressibility has a more significant effect on permeability estimation.

4.5 Sensitivity of Differential Pressure to Langmuir Pressure and Langmuir Volume

Using the values from Table 2 with systematic values of Langmuir pressure and Langmuir volume with differential pressure to study these effects on the estimation of permeability. The investigation is with Langmuir pressure ranging from $100\ psi$ to $450\ psi$ and Langmuir volume ranging from $800\ scf/ton$ to $1300\ scf/ton$. Figures 15 and 16 show that curves of different Langmuir pressures or Langmuir volumes merge into a single curve. Estimated permeability changes a little for different values of Langmuir pressures or Langmuir volumes. The estimated permeability is accurate because varying Langmuir pressures and/or Langmuir volumes have a lesser impact.

With an increasing amount of gas, the corresponding pore pressure increases. The adsorptive characteristics of carbon dioxide are higher relative to its high Langmuir volume and low Langmuir pressure than that of Helium and Methane. The high Langmuir Volume and low Langmuir pressure would impact the analytical solution, thereby giving a less accurate permeability estimation.

Simulated pressure means the endmost equilibrium pressure for each pressure step and typifies similar pressure to determine permeability.

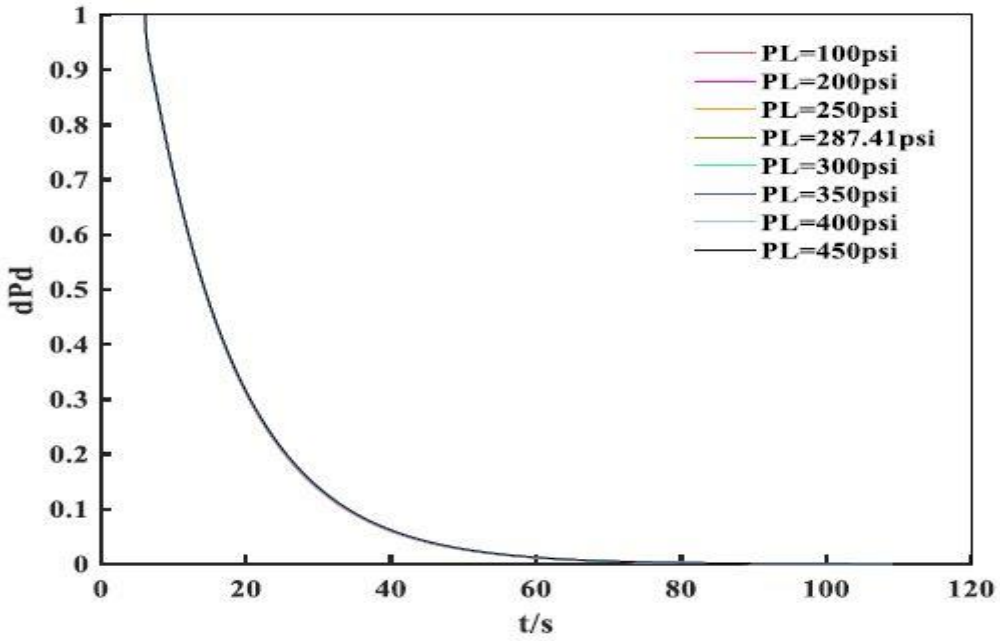

Figure 14: Differential Pressure for various Langmuir pressures.

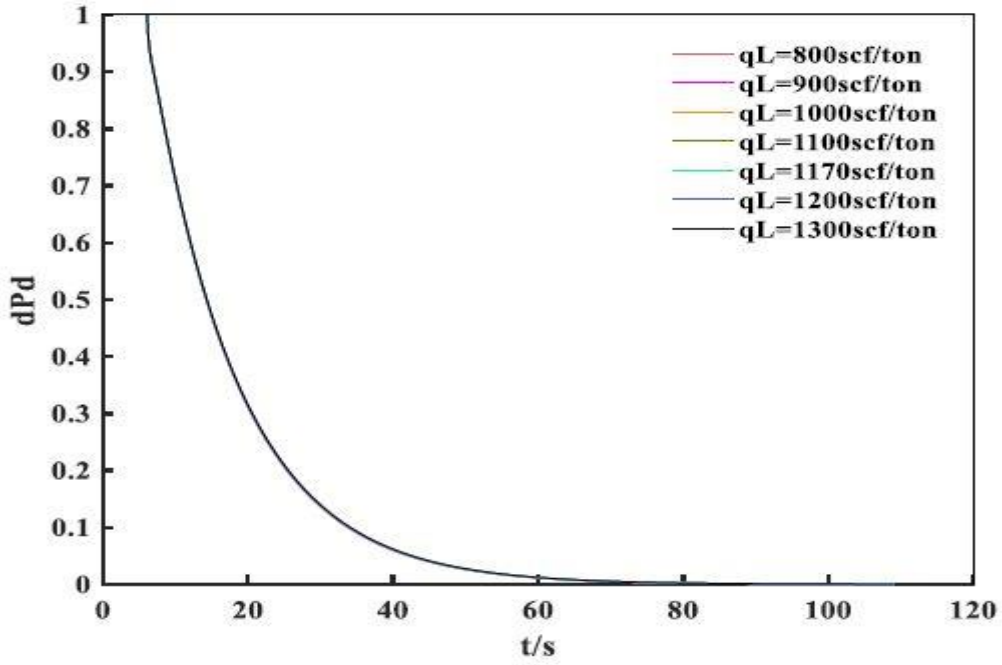

Figure 15: Differential pressures for various Langmuir volumes.

Simulated pressure means the endmost equilibrium pressure for each pressure step and typifies similar pressure to determine permeability.

Chapter Five

Conclusion

The estimation of permeability in unconventional reservoirs is by the pressure pulse decay method. This research method uses an integrated approach of experimental and simulated methods to determine permeability from the pressure profile. A simulation approach centered on solving the governing model equation of pressure-dependent variables to affirm the simulated pressure outline. This study's outcomes show a related trend of permeability transformation, but with enhanced permeability outcomes as against analytical solutions. The enhanced permeability is related to the two-stage approach of constant gas properties for an analytical solution. An analytical solution of permeability acquired from simulation and experimental pressure outlines. The approach in this study is using history matching of simulated and experimental pressure outlines. From this study, the following assertions exist:

1. With a reduction in the effective stress, permeability estimation with helium increases with increasing pressure. Different adsorptive gases depict different permeability responses. Permeability increases as an effective stress decrease for methane gas are higher than matrix swelling caused by sorption induction. Carbon dioxide exhibits two different patterns such that with dominant sorption effect, permeability reduces, but as effective stress reduces, then permeability begins to increase. For pressure below 110 psi, carbon dioxide is the highest permeability, but at above 150 psi, helium is the highest permeability.
2. Based on the initial approach variance, there is no effect on permeability, even with a higher pressure. Even at low pressure, the same trend occurred. The variance between pressure along the sample for the three gases at all pressure steps for gas properties is little or negligible.
3. Based on the next approach variance, there is a more significant influence on permeability. The history matching approach gives a better estimation of permeability as against pressure outlines of simulated and experimental.
4. The systematic investigation of the effects of variations of porosity, gas compressibility, Langmuir pressure, and Langmuir volume indicated that estimated permeability was based on the changing values of the intrinsic factors.

Simulated pressure means the endmost equilibrium pressure for each pressure step and typifies similar pressure to determine permeability.

References

Aljamaan, H. A. (2013). In-Depth Experimental Investigation of Shale Physical and Transport Properties. doi:doi:10.1190/urtec2013-114

Alnoaimi, K., & Kovscek, A. (2013). Experimental and numerical analysis of gas transport in shale including the role of sorption. . *SPE Annu. Tech. Conf. Exhib. SPE 166375*. doi:10.2118/166375-MS

Amaefule, J., Wolfe, K., Walls, J., Ajufo, A., & Peterson, E. (1986). Laboratory determination of effective liquid permeability in low-quality reservoir rocks by the pulse decay technique. *SPE California Regional Meeting, 2-4 April, Oakland, California*. doi:10.2118/15149-MS

American Petroleum Institute, A. (1998). Recommended Practices for Core Analysis. *American Petroleum Institute (API)*.

Berg, R. (1970). Method For Determining Permeability From Reservoir Rock Properties.

Beskok, A., & Karniadakis, G. E. (1999). A MODEL FOR FLOWS IN CHANNELS, PIPES, AND DUCTS AT MICRO AND NANO SCALES. *Microscale ThermoPhysical Engineering, 3*(1). Retrieved from https://doi.org/10.1080/108939599199864

Brace, W., Walsh, J., & Frangos, W. (1968). Permeability of granite under high pressure. *Journal geophysics Research and Space Physics, 73*, 2225-2236.

Cipolla, C., & Lolon, E. (2010). Reservoir Modelling in Shale Gas Reservoirs.

Civan, F., Rai, C. S., & Sondergeld, C. H. (2011). Shale-gas permeability and diffusivity inferred by the improved formulation of relevant retention and transport mechanisms. Transport in Porous Media. doi: 86839:925-944

Cui, X., Bustin, A., & Bustin, R. (2009). Measurements of gas permeability and diffusivity of tight reservoir rocks: Different approaches and their applications. . *Geofluids , 9* , 208–223. doi:10.11117j.1468-8123.2009.00244.x

Darabi, H., Ettehad, A., & Javadpour, F. (2012). Gas flow in ultra-tight shale strata. *Journal of Fluid Mechanics,, 710*, 641-658.

Darcy, H. (1856). *Les fontaines publiques de la ville de Dijon. Paris: Dalmont*.

Dicker, A., & Smits, R. (1988). A Pratical approachfor determining permeability from laboratory pressure-pulse decay measurements. *SPE*. doi:10.2118/17578-MS

Finsterle, S., & Persoff, P. (1997). Determining permeability of tight rock samples using inverse modeling. *Water Resources Research, 33*, 1803–1811.

Han, G., Chen, Y., Liu, M., & Liu, X. (2019). Differneces in Performance of Models for Heterogeneous Cores during Pulse Decay Tests. *Applied Science, 9*, 3206.

Hsieh, P., Tracy, J. V., Neuzil, C., Bredehoeft, J., & Silliman, S. (1981). A transient laboratory method for determining the hydraulic properties of "tight" rocks-I. *Int. J. Rock Mech. Min. Sci. Geomech. Abstr. , 18*, 245–252. doi:10.1016/0148-9062(81)90979-7

Javadpour. (2009). Nanopores and apparent permeability of gas flow in mudrocks (shales and siltstone). *Journal of Canadian Petroleum Technology, 48*(8), 16-21.

Simulated pressure means the endmost equilibrium pressure for each pressure step and typifies similar pressure to determine permeability.

Javadpour, F. (2009). Nanopores and apparent permeability of gas flow in mudrocks (shales and siltstone). *Journal of Canadian Petroleum Technology., 48*, 16–21.

Javadpour, F., Fisher, D., & Unsworth, M. (2007). Nanoscale Gas Flow in Shale Gas Sediments. *Journal of Canadian Petroleum Technology, 46*.

Jia, B., Tsau, J.-S., & Barati, R. (2018). Different Flow Behaviorsnof Low-Pressure and High-Pressure Carbon Dioxide in Shales. *SPE Journal, 23*, 1452-1468.

Jones, S. (1997). A Technique for Faster Pulse-Decay Permeability Measurements in Tight Rocks. *12*, 19–26. doi:doi:10.2118/28450-PA

Kamath, J., Boyer, R., & Nakagwa, F. (1992). Characterization of Core Scale Heterogeneities using Laboratory Pressure Transients. *SPE Formation Evaluation, 7*, 219-227.

Knudsen, M. (1909). *Ann. Phys., Lpz, 28*, 75 – 130.

Langmuir, I. (1916). The constitution and fundamental properties of solids and liquids, ,. *Journal of American Chemical Society, 38* (11). doi:2221-2295.1916

Liehui, Z. (2019). Well Production Performance Analysis for Shale Gas Reservoirs. *Develoments in Petroleum Science, Elsevier, 66*. doi:10.1016/B978-0-444-64315-5.00001-2.

Loucks, R. G., Reed, R. M., Ruppel, S. C., & Jarvie, D. M. (2009). Morphology, genesis, and distribution of nanometer-scale pores in siliceous mudstones of the Mississippian Barenett Shale. *Journal of Sedeimentary Research, 79*(12), 848-861.

Michel, Villazon, G., R., S., Civian, F., & Devegowda, D. (2011). Parametric Investigation of Shale Gas Production Considering Nano-Scale Pore Size Distribution, Formation Factor, and Non-Darcy Flow Mechanisms.

Moghanloo, R. G., Javadpour, F., & Davudou, D. (2013). Contibution of Methane Molecule Diffusion in Kerogen to Gas-in-Place and Production. . *SPE Western Regional & AAPG Pacific Section Meeting 2013 Joint Technical Conference*.

Ning, X. (1992, June 20). The measurement of matrix and fracture Properties in Naturally Fracture Low Permeability Cores Using a Pressure Pulse Method. Texas, Texas, USA.

Peaceman, D. (1977). Fundamentals of Numerical Reservoir Simulation. *6*.

Sakhaee-Pour, A., & Bryant, S. (2012). Gas Permeability of Shale. *Society of Petroleum Engineers*. doi: doi:10.2118/146944-PA

Swanson, B. (1981). A simple correlation betweem permeability and mercury pressure curve. *Journal of Petroleum Technology, 27*, 2498-2504.

Tanikawa, W., & Shimamoto, T. (2009). Correction to ''comparison of Klinkenberg-corrected gas pemeability and wate pemeability in sdimntary rocks''. *International Journal of Rock Mechanics and Mining Science, 46*, 1394-1395.

U.S. Energy Information Agency, E. (2019). *U.S. Energy Information Agency, EIA.,(2019) Annual Energy Outlook.*

Simulated pressure means the endmost equilibrium pressure for each pressure step and typifies similar pressure to determine permeability.

Wang, H., & Marongiu-Porcu, M. (2015). Impact of Shale-gas Apparent Permeability on Production: Combined Effects of Non-Darcy Flow/Gas-Slippage, Desoprtion, and Geomechanics. *Society of Petroleume Engineers*. doi:10.2118/173196-PA

Wang, Y., Liu, S., & Elsworth, D. (2015). Laboratory investigations of gas flow behaviors in tight anthracite and evaluation of different pulse-decay methods on permeability estimation. *Int. J. Coal Geol., 149*, 118–128. doi:doi:10.1016/j.coal.2015.07.009

Xu, B., Haghighi, M., & Cooke, D. (2012). Production Data Analysis in Eagle Ford Shale gas Reservoir. *Society of Petroleum Engineer*.

Ziarani, A. S., & Aguilera, R. (2012). Transp Porous Media. Retrieved from https//doi.org/10.1007/s11242-011-9842-6

Simulated pressure means the endmost equilibrium pressure for each pressure step and typifies similar pressure to determine permeability.

Appendix

1.1 Matrix Formulation

$$\begin{bmatrix} -\left[\left(\frac{\phi}{RT\Delta tZ}\right)_1^{n+1(r)} + \left(\frac{k\rho}{\mu\Delta x^2}\right)_{1+\frac{1}{2}}^{n+1(r)} + \left(\frac{k\rho}{\mu\Delta x^2}\right)_{1-\frac{1}{2}}^{n+1(r)}\right] & \left(\frac{k\rho}{\mu\Delta x^2}\right)_{1+\frac{1}{2}}^{n+1(r)} & 0 & 0 \dots\dots\dots 0 & 0 \\ \left(\frac{k\rho}{\mu\Delta x^2}\right)_{2-\frac{1}{2}}^{n+1(r)} & -\left[\left(\frac{\phi}{RT\Delta tZ}\right)_2^{n+1(r)} + \left(\frac{k\rho}{\mu\Delta x^2}\right)_{2+\frac{1}{2}}^{n+1(r)} + \left(\frac{k\rho}{\mu\Delta x^2}\right)_{2-\frac{1}{2}}^{n+1(r)}\right] & \left(\frac{k\rho}{\mu\Delta x^2}\right)_{2+\frac{1}{2}}^{n+1(r)} & 0 \dots\dots..0 & 0 \\ 0 & \left(\frac{k\rho}{\mu\Delta x^2}\right)_{3-\frac{1}{2}}^{n+1(r)} & -\left[\left(\frac{\phi}{RT\Delta tZ}\right)_3^{n+1(r)} + \left(\frac{k\rho}{\mu\Delta x^2}\right)_{3+\frac{1}{2}}^{n+1(r)} + \left(\frac{k\rho}{\mu\Delta x^2}\right)_{3-\frac{1}{2}}^{n+1(r)}\right] & \left(\frac{k\rho}{\mu\Delta x^2}\right)_{3+\frac{1}{2}}^{n+1(r)} & 0 \dots\dots..0 & 0 \\ & & \vdots & & & \\ 0 & 0 & 0 & \left(\frac{k\rho}{\mu\Delta x^2}\right)_{N_x-\frac{1}{2}}^{n+1\ (r)} & -\left[\left(\frac{\phi}{RT\Delta tZ}\right)_{N_x}^{n+1(r)} + \left(\frac{k\rho}{\mu\Delta x^2}\right)_{N_x+\frac{1}{2}}^{n+1\ (r)} + \left(\frac{k\rho}{\mu\Delta x^2}\right)_{N_x-\frac{1}{2}}^{n+1\ (r)}\right] \end{bmatrix} \begin{bmatrix} P_1^{n+1\ (r+1)} \\ P_2^{n+1\ (r+1)} \\ P_3^{n+1\ (r+1)} \\ \vdots \\ P_{N_x}^{n+1\ (r+1)} \end{bmatrix}$$

$$= \begin{bmatrix} -\frac{\phi}{RT\Delta t}\left(\frac{P}{Z}\right)_1^n + (1-\phi)\frac{C_1^{n+1\ (r)} - C_1^n}{\Delta t} - \left(\frac{k\rho}{\mu\Delta x^2}\right)_{1-\frac{1}{2}}^{n+1(r)} * P_u^{n+1} \\ -\frac{\phi}{RT\Delta t}\left(\frac{P}{Z}\right)_2^n + (1-\phi)\frac{C_2^{n+1\ (r)} - C_2^n}{\Delta t} \\ -\frac{\phi}{RT\Delta t}\left(\frac{P}{Z}\right)_3^n + (1-\phi)\frac{C_3^{n+1\ (r)} - C_3^n}{\Delta t} \\ \vdots \\ -\frac{\phi}{RT\Delta t}\left(\frac{P}{Z}\right)_{N_x}^n + (1-\phi)\frac{C_{N_x}^{n+1\ (r)} - C_{N_x}^n}{\Delta t} - \left(\frac{k\rho}{\mu\Delta x^2}\right)_{N_x+\frac{1}{2}}^{n+1\ (r)} * P_d^{n+1} \end{bmatrix}$$

1.2 linearization of model

$$F_m(P_i, P_{i+1}, P_{i-1}, P_{N_x}) = \left(\frac{\phi}{RT\Delta tZ}\right)_1^{n+1(r)} - \left[\left(\frac{\phi}{RT\Delta tZ}\right)_1^{n+1(r)} + \left(\frac{k\rho}{\mu\Delta x^2}\right)_{1+\frac{1}{2}}^{n+1(r)} + \left(\frac{k\rho}{\mu\Delta x^2}\right)_{1-\frac{1}{2}}^{n+1(r)}\right] +$$

$$\left(\frac{k\rho}{\mu\Delta x^2}\right)_{1+\frac{1}{2}}^{n+1(r)} - \frac{\phi}{RT\Delta t}\left(\frac{P}{Z}\right)_1^n + (1-\phi)\frac{C_1^{n+1\ (r)} - C_1^n}{\Delta t} - \left(\frac{k\rho}{\mu\Delta x^2}\right)_{1-\frac{1}{2}}^{n+1(r)} * P_u^{n+1} + -\frac{\phi}{RT\Delta t}\left(\frac{P}{Z}\right)_1^n +$$

$$(1-\phi)\frac{C_1^{n+1\ (r)} - C_1^n}{\Delta t} - \left(\frac{k\rho}{\mu\Delta x^2}\right)_{1-\frac{1}{2}}^{n+1(r)} * P_d^{n+1} = 0$$

Simulated pressure means the endmost equilibrium pressure for each pressure step and typifies similar pressure to determine permeability.

Linearization of F_m

$$\frac{{F_m}^n}{\partial P_i}{\Delta P_i}^n + \frac{{F_m}^n}{\partial P_{i+1}}{\Delta P_{i+1}}^n + \frac{{F_m}^n}{\partial P_{i-1}}{\Delta P_{i-1}}^n + \frac{{F_m}^n}{\partial P_{N_x}}{\Delta P_{N_x}}^n + {F_m}^n$$

1.3 Flow Charts

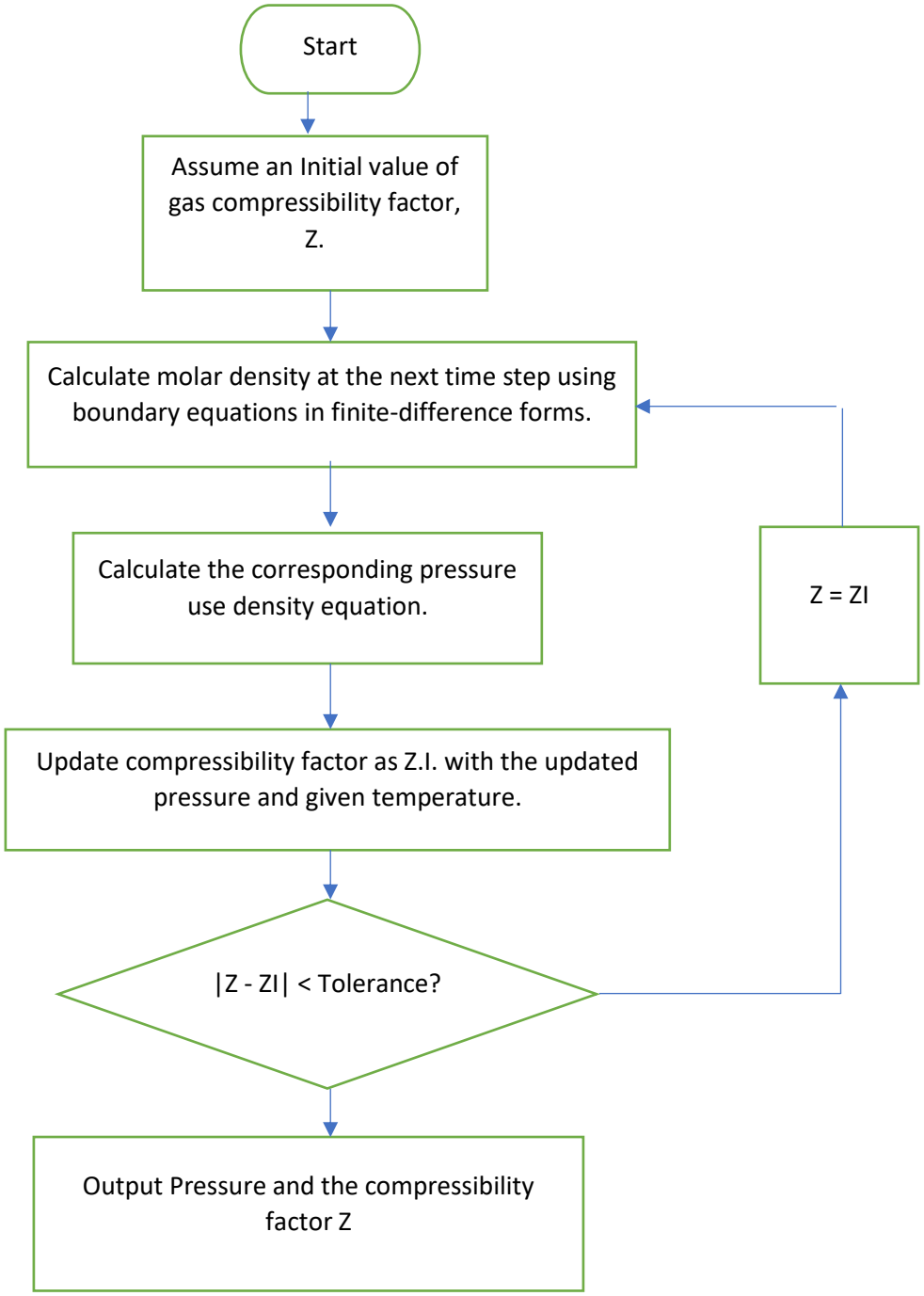

Figure A- 1: Flowchart for the conversion of density to pressure

Simulated pressure means the endmost equilibrium pressure for each pressure step and typifies similar pressure to determine permeability.

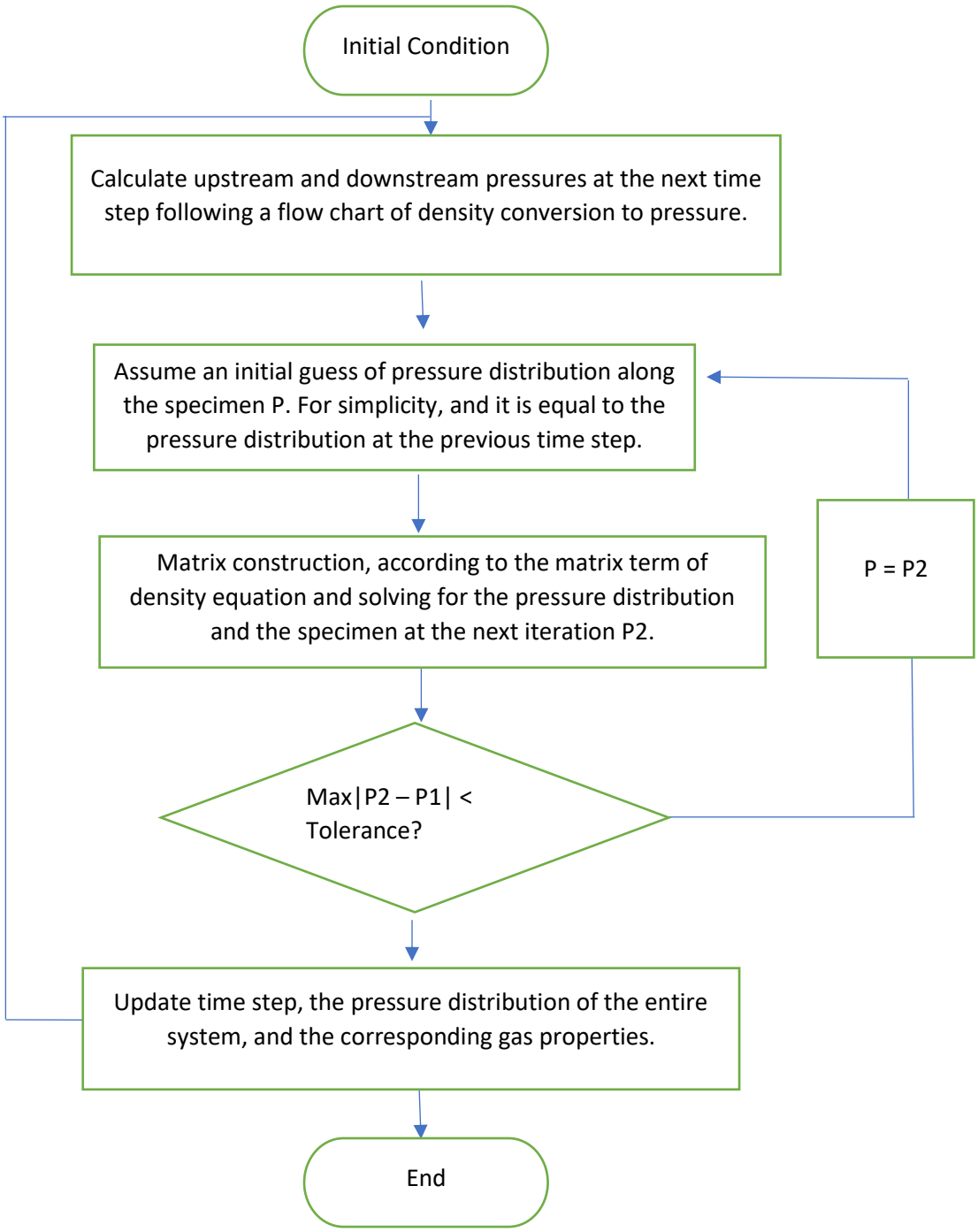

Figure A- 2: Flow Chart for implementation of the numerical simulation procedure

Simulated pressure means the endmost equilibrium pressure for each pressure step and typifies similar pressure to determine permeability.